Title: Impacts of vaccination and Severe Acute Respiratory Syndrome Coronavirus 2 variants Alpha and Delta on Coronavirus Disease 2019 transmission dynamics in four metropolitan areas of the United States

Running Title: Impacts of COVID-19 vaccination and SARS-CoV-2 variants

One-Sentence Summary: Using a compartmental model parameterized to reproduce available reports of new Coronavirus Disease 2019 (COVID-19) cases, we quantified the impacts of vaccination and Severe Acute Respiratory Syndrome Coronavirus 2 (SARS-CoV-2) variants Alpha (lineage B.1.1.7) and Delta (lineage B.1.617.2) on regional epidemics in the metropolitan statistical areas (MSAs) surrounding Dallas, Houston, New York City, and Phoenix.

Authors: Abhishek Mallela[1], Ye Chen[1], Yen Ting Lin, Ely F. Miller, Jacob Neumann, Zhili He, Kathryn E. Nelson, Richard G. Posner, William S. Hlavacek*

[1]These authors contributed equally.

Corresponding author. Email: wish@lanl.gov

Address for correspondence: William S. Hlavacek, Theoretical Biology and Biophysics Group, Theoretical Division, Los Alamos National Laboratory, Los Alamos, NM 87545, USA.

Affiliations: Los Alamos National Laboratory, Los Alamos, New Mexico, USA (W.S. Hlavacek, Y.T. Lin, A. Mallela); Northern Arizona University, Flagstaff, Arizona, USA (Y. Chen, Z. He, E.F. Miller, K.E. Nelson, J. Neumann, R.G. Posner).

ABSTRACT

To characterize Coronavirus Disease 2019 (COVID-19) transmission dynamics in each of the metropolitan statistical areas (MSAs) surrounding Dallas, Houston, New York City, and Phoenix in 2020 and 2021, we extended a previously reported compartmental model accounting for effects of multiple distinct periods of non-pharmaceutical interventions by adding consideration of vaccination and Severe Acute Respiratory Syndrome Coronavirus 2 (SARS-CoV-2) variants Alpha (lineage B.1.1.7) and Delta (lineage B.1.617.2). For each MSA, we found region-specific parameterizations of the model using daily reports of new COVID-19 cases available from January 21, 2020 to October 31, 2021. In the process, we obtained estimates of the relative infectiousness of Alpha and Delta as well as their takeoff times in each MSA (the times at which sustained transmission began). The estimated infectiousness of Alpha ranged from 1.1x to 1.6x that of viral strains circulating in 2020 and early 2021. The estimated relative infectiousness of Delta was higher in all cases, ranging from 1.6x to 2.2x. The estimated Alpha takeoff times ranged from February 16 (for New York City, which was evidently impacted much earlier than the other regions) to April 2, 2021. The estimated Delta takeoff times were more tightly clustered, ranging from June 15 to June 24, 2021. Estimated takeoff times are consistent with genomic surveillance data.

Keywords: Coronavirus Disease 2019 (COVID-19), Severe Acute Respiratory Syndrome Coronavirus 2 (SARS-CoV-2), vaccination, SARS-CoV-2 variant Alpha (lineage B.1.1.7), SARS-CoV-2 variant Delta (lineage B.1.617.2), mathematical model, Bayesian inference

INTRODUCTION

In 2020, Coronavirus Disease 2019 (COVID-19) transmission dynamics were significantly influenced by non-pharmaceutical interventions [1–7]. In 2021, other factors arose with significant impacts on disease transmission, namely, vaccination [8–9] and emergence of Severe Acute Respiratory Syndrome Coronavirus 2 (SARS-CoV-2) variants [10–11].

Mass vaccination in the United States (US) began on December 14, 2020 [12], with demonstrable reduction of disease burden within vaccinated populations [13]. As the vaccination campaign progressed into March 2021, there was widespread reduction in disease incidence [14] and relaxation of state-mandated non-pharmaceutical interventions [15].

In early 2021, SARS-CoV-2 variant Alpha (lineage B.1.1.7) spread across the US and became the dominant circulating strain [16]. By the end of July 2021, the Delta variant (lineage B.1.617.2) had supplanted Alpha [17], concomitant with increases in new COVID-19 case detection [14]. Both Alpha and Delta have been estimated to be more transmissible than strains circulating earlier [18–23], and it was determined that vaccinated persons infected with Alpha and Delta were capable of transmitting disease [24, 25].

In earlier work, with the aid of a compartmental model, we quantified the impact of non-pharmaceutical interventions on COVID-19 transmission dynamics [5–7]. We found that the multiple surges in disease incidence seen in 2020 [14] could be explained by changes in protective disease-avoiding behaviors, which we will refer to collectively as social distancing. Here, to quantify the impacts of vaccination and SARS-CoV-2 variants Alpha and Delta on COVID-19 transmission dynamics, we extended the model of Lin et al. [5] by adding consideration of vaccination and variants with increased transmissibility. We then found region-

specific parameterizations of the model using vaccination and surveillance case data available for the MSAs surrounding Dallas, Houston, New York City, and Phoenix.

METHODS

Data

Daily reports of new confirmed COVID-19 cases were obtained from the GitHub repository maintained by The New York Times newspaper [26]. Daily reports of newly completed vaccinations were obtained from the Covid Act Now database [27]. County-level surveillance and vaccination data were aggregated to obtain daily case and vaccination counts for the MSAs surrounding Dallas, Houston, New York City, and Phoenix. In the case of a missing daily report, we imputed the missing information as described in the Appendix.

Compartmental Model for Disease Transmission Dynamics

We used the compartmental model illustrated in Figure 1 (and Appendix Figure 1) to analyze data available for each MSA of interest. The model consists of ordinary differential equations (ODEs) describing the dynamics of 40 populations (state variables) (Appendix Equations 1–38). The state variables are each defined in Appendix Table 1. Model parameters are defined in Tables 1–3. Key features of the model are described below, and a full description of the model is provided in the Appendix.

We extended the model of Lin et al. [5] by including 15 new populations and 28 new transitions. The new compartments and transitions, which are highlighted in Figure 1, capture vaccination among susceptible persons, recovered persons and infected non-quarantined persons without symptoms at a time-varying *per capita* rate $\mu(t)$. The value of $\mu(t)$ changes daily for

86 consistency with MSA-specific daily reports of completed vaccinations (Appendix Equation 37)
87 from the COVID Act Now database. The model also captures immune responses to vaccination
88 yielding varying degrees of protection and consequences of breakthrough infection of vaccinated
89 persons. Vaccine protection against transmissible infection was taken to be variant-dependent.

90 We introduced a dimensionless step function, denoted $Y_\theta(t)$ (Appendix Equation 38),
91 which multiplies the disease-transmission rate constant β to account for m variants. In this study,
92 $m = 2$ (see Appendix Equations 1–4, 18–22, and 24). Thus, in the new model, the quantity
93 $Y_\theta(t)\beta$ (vs. β alone) characterizes disease transmissibility at time t. The step function $Y_\theta(t)$ was
94 initially assigned a value of $y_0 = 1$, and the value of $Y_\theta(t)$ was allowed to increase at times $t =$
95 θ_1 and $t = \theta_2$ (Appendix Equation 38). The disease transmission rate constant of the Alpha
96 variant was considered by introducing a step increase from $y_0\beta \equiv 1\beta$ to $y_1\beta$ (with $y_1 > 1$) at
97 time $t = \theta_1$ (the Alpha takeoff time). Similarly, the disease transmission rate constant of the
98 Delta variant was considered by introducing a step increase from $y_1\beta$ to $y_2\beta$ (with $y_2 > y_1$) at
99 time $t = \theta_2 > \theta_1$ (the Delta takeoff time). We will refer to y_1 and y_2 as the Alpha and Delta
100 transmissibility factors, respectively.

101 As in the original model of Lin et al. [5], the extended model accounts for a series of $n +$
102 1 distinct social-distancing periods (an initial period and n additional periods). Social-distancing
103 periods are characterized by two step functions: $P_\tau(t)$ and $\Lambda_\tau(t)$. The values of these functions
104 change coordinately at a set of times $\tau = (\sigma, \tau_1, \ldots, \tau_n)$ (Appendix Equations 35 and 36), where
105 σ is the start time of the initial social-distancing period and τ_i is the start time of the ith social-
106 distancing period after the initial social-distancing period. The values of $P_\tau(t)$ and $\Lambda_\tau(t)$ are zero
107 before time $t = \sigma$. The value of $P_\tau(t)$ defines the steady-state setpoint fraction of the susceptible

population practicing social distancing at time t, and the value of $\Lambda_\tau(t)$ defines a time scale for establishment of the steady state. The value of $\Lambda_\tau(t)$ is an eigenvalue equal to a sum of social-distancing rate constants *(5)*. The non-zero values of $P_\tau(t)$ and $\Lambda_\tau(t)$ are denoted $p_0, \ldots, p_n$ and $\lambda_0, \ldots, \lambda_n$. We assume that vaccinated persons do not practice social-distancing. Recall that we use the term "social-distancing" to refer to behaviors adopted to protect against infection. These behaviors are assumed to reduce the risk of infection by a factor m_b.

Parameters

As indicated in Tables 1 and 2, we used MSA-specific case reporting data available up to October 31, 2021 to infer MSA-specific values for parameters characterizing the start time of the local epidemic (t_0), local disease transmissibility of ancestral viral strains (β), local social-distancing dynamics (σ, λ_0, p_0, τ_i, λ_i and p_i, for $i = 1, \ldots, n$), local emergence of variants (θ_1, y_1, θ_2, y_2), the local rate of new case detection (f_D), and noise in local case detection and reporting (r). Values for other parameters were fixed (Table 3); inferences are conditioned on these fixed parameter estimates. There are 18 fixed parameters taken to be applicable for all MSAs. The total regional population S_0, which is taken to be fixed, was set on the basis of census data. The real-time *per capita* vaccination rate $\mu(t)$, a piecewise linear function, was set for consistency with the current empirical *per capita* rate of vaccination [27]. We adopted the fixed parameter estimates of Lin et al. [5]. New fixed parameter estimates made in this study for m_h, f_0, f_1, f_2, and k_V are explained in the Appendix. The m_h parameter characterizes vaccine protection against severe disease, the f_0, f_1, and f_2 parameters account for differential vaccine effectiveness against the three viral strains considered in this study (ancestral, Alpha, and Delta), and the k_V parameter characterizes the waiting time between vaccination and the acquisition of

vaccine-induced immunity. Our model does not account for gradual loss of immunity over time. We let $\tilde{\mu}(t) = \mu_i$ for times t throughout the ith day after January 21, 2020 (Appendix Equation 37), where μ_i is the fraction of the local population reported to complete vaccination over the 1-d surveillance period [27]. We then defined $\mu(t)$ as the piecewise linear interpolant to $\tilde{\mu}(t)$. In summary, for a given inference, the number of adjustable parameters was $2m + 3n + 5$, where m is the number of variants under consideration ($m = 2$ in this study) and n is the number of distinct social-distancing periods being considered beyond an initial social-distancing period. The setting for n was determined through a model-selection procedure described in the Appendix.

Auxiliary Measurement Model

We assumed that state variables of the compartmental model (Figure 1, Appendix Table 1) are related to the expected number of new cases reported on a given calendar date through an auxiliary measurement model (Appendix Equations 39 and 40). The measurement model has one parameter: f_D, the region-specific fraction of new symptomatic infections detected. Thus, $f_D \in [0, 1]$. As a simplification, we considered f_D to be time-invariant. This simplification means that we assumed, for example, that case detection was neither limited nor strongly influenced by testing capacity, which varied over time. This assumption is reasonable if, for example, case detection is mainly determined by presentation for testing and, moreover, the motivations and societal factors that influence presentation remained roughly constant over the period of interest. One can also interpret f_D as the time-averaged case detection rate. The measurement-model parameter f_D was inferred jointly with the adjustable model parameters and the likelihood parameter r (see below).

Statistical Model for Noise in Case Detection and Reporting

We assumed that noise in new case detection and reporting on the ith day after January 21, 2020 is captured by a negative binomial distribution $\mathrm{NB}(r, q_i)$ centered on $I(t_i, t_{i+1})$, the expected number of new cases detected over the ith day after January 21, 2020 as given by the compartmental model and the auxiliary measurement model (Appendix Equations 1–40). These and other assumptions led to the likelihood function used in inference (Appendix Equations 41–43). We determined the probability parameter q_i in $\mathrm{NB}(r, q_i)$ using Appendix Equation 43; the dispersion parameter r was taken to be a time-invariant adjustable parameter applicable for all days of case reporting. The likelihood parameter r was inferred jointly with the adjustable model parameters and the adjustable measurement-model parameter f_D.

Computational Methods

We determined the intervals of the step functions $Y_\theta(t)$, $P_\tau(t)$, and $\Lambda_\tau(t)$ (i.e., θ and τ) using a model-selection procedure described in the Appendix. Simulations and Bayesian inferences were performed as previously described [5–7] and in the Appendix. Files needed to reproduce inferences using the software package PyBioNetFit [28] are available online (https://github.com/lanl/PyBNF/tree/master/examples/Vax_and_Variants). The files include case data, vaccination data, and diagnostic plots related to Bayesian inference using Markov chain Monte Carlo (MCMC) sampling. Summary diagnostics characterizing the sampling for each MSA are given in Table 4. The results of Table 4 indicate that sampling was acceptable.

RESULTS

In earlier work, we demonstrated that new COVID-19 case detection over various periods in 2020 can be faithfully reproduced for 280 (out of the 384) metropolitan statistical areas

(MSAs) in the US and all 50 states by region-specific parameterizations of a compartmental model that accounts for time-varying non-pharmaceutical interventions [5–7]. However, in 2021, the model lost its ability to capture disease transmission dynamics, presumably because of the impacts of vaccination and the emergence of more transmissible SARS-CoV-2 variants, namely, Alpha and Delta. To remedy this problem, we accounted for these factors in an extension of the model of Lin et al. [5] (Figure 1). Details about the model extension are provided in the Appendix. We used the new model to analyze data available for four MSAs (Figures 2–5).

As illustrated in Figures 2A, 3A, 4A, and 5A for the Dallas, Houston, New York City, and Phoenix MSAs respectively, the new model is able to explain surveillance case data over the period starting on January 21, 2020 and ending on October 31, 2021. The surveillance case data—daily reports of newly detected COVID-19 cases—for each of the 4 MSAs of interest largely lie within the 95% credible interval of the posterior predictive distribution for new case detection, which indicates that each regional model has explanatory power for the period of interest.

Each regional model (parameterized to reproduce MSA-specific case reports) provides insight into the impacts of social-distancing behaviors and the emergence of the Alpha and Delta variants; compare panel A and the corresponding panel B in Figures 2–5. For example, as can be seen in Figure 4A, the New York City MSA experienced four notable surges in disease incidence over the period of interest. Figure 4B suggests that the first surge ended because of adoption of social-distancing behaviors, the second surge occurred because of relaxation of social-distancing behaviors, the third surge was caused by Alpha, and the fourth surge was caused by Delta. Interestingly, in other MSAs, Alpha had relatively little impact on disease incidence (compare Figures 4A and 4B to Figures 2A and 2B, 3A and 3B, and 5A and 5B). This difference is partly

attributable to the later arrival of Alpha in the Dallas, Houston, and Phoenix MSAs in combination with the progress of mass vaccination, which is tracked locally in panel C of Figures 2–5.

On the basis of our region-specific parameterizations, we estimated the immune and susceptible fractions of each MSA population, as well as the fractions that achieved immunity through infection and/or vaccination (see panel C in Figures 2–5). Each of these panels shows the time evolution of five different populations in an MSA. In each MSA, only a minority of the population remained susceptible to infection (with Delta) on October 31, 2021, with a sizable fraction of the susceptible population being protected to a degree against severe disease by having completed vaccination.

Our inferences provide quantitative insights into the increased transmissibility of Alpha and Delta (y_1 and y_2) and their takeoff times (θ_1 and θ_2) in each of the 4 MSAs of interest. Figure 6 shows the marginal posteriors of y_1, y_2, θ_1, and θ_2, which were found on the basis of surveillance data for each MSA (daily case counts) reported between January 21, 2020 and October 31, 2021. Maximum *a posteriori* (MAP) estimates and 95% credible intervals for θ_1 and θ_2 for each MSA are also shown in Figure 6. The MAP estimates for y_1 range from 1.1 (for the Dallas MSA) to 1.6 (for the Phoenix MSA). The MAP estimates for y_2 range from 1.6 (for the Dallas MSA) to 2.2 (for the New York City MSA). The MAP estimates for θ_1 range from February 16, 2021 (for the New York City MSA) to April 2, 2021 (for the Phoenix MSA). The New York City MSA was impacted much earlier than the other MSAs by Alpha. The MAP estimates for θ_2 range from June 15, 2021 (for the New York City MSA) to June 24, 2021 (for the Dallas MSA). The estimated takeoff times are consistent with regional genomic surveillance data [30], which are summarized by the shaded regions of panel A in Figures 2–5.

DISCUSSION

We extended a model for COVID-19 transmission dynamics that already incorporated time-varying changes in non-pharmaceutical interventions [5] to include the effects of vaccination and new variants. This model together with its region-specific parameterizations based on case data available through October 31, 2021 provide quantitative insights into the relative infectiousness of SARS-CoV-2 variants Alpha (lineage B.1.1.7) and Delta (lineage B.1.617.2). The increased transmissibility of Alpha and Delta in comparison to ancestral strains is characterized by the marginal posteriors for the transmissibility factors y_1 and y_2 shown in Figure 6 (panels A, C, E, and G). The maximum *a posteriori* (MAP) estimates of the transmissibility factors were similar across the four metropolitan statistical areas (MSAs) of interest (centered on Dallas, Houston, New York City, and Phoenix). The averages of our y_1 and y_2 MAP estimates indicate that Alpha was 1.3x more infectious than ancestral strains, whereas Delta was 2.0x more infectious (corresponding to Delta being 54% more infectious than Alpha). These estimates are consistent with estimates provided in other studies [18–23]. This information combined with our earlier estimates of MSA-specific basic reproduction numbers [7] indicate that Delta is among one of the most infectious viruses known. We obtain an R_0 estimate of 16 for the New York City MSA.

We also obtained estimates of precisely when sustained transmission of Alpha and Delta began in each of the four MSAs. The takeoff times are characterized by the marginal posteriors for θ_1 and θ_2 shown in Figure 6 (panels B, D, F, and H). The takeoff times are similar across the MSAs except that the New York City MSA was evidently impacted much earlier by Alpha: circa February 16, 2021 vs. circa late March to early April 2021 for the other MSAs. The estimated takeoff times are consistent with the observed prevalence of Alpha and Delta sequences detected

in regional genomic surveillance [30], as can be seen by comparing the two shaded regions in panel A of Figures 2–5 against the changes in transmissibility $Y_\theta(t)$ depicted in the corresponding panel B of Figures 2–5. It should be noted that the case data shown in Figures 2–5 are from the MSAs of interest (through aggregation of county-level data), whereas the genomic surveillance data are from larger regions.

Our study has notable limitations, starting with the obvious uncertainties related to model assumptions and fixed parameter estimates, which are discussed in some detail in the Appendix. For example, our model neglects gradual loss of sterilizing immunity over time and assumes a constant rate of case detection. Moreover, we caution that the inference jobs performed in this study were challenging because of the relatively high-dimensional parameter spaces involved (in comparison to typical inferences involving an ODE model-constrained likelihood function). Diagnostics indicate good sampling (Table 4, https://github.com/lanl/PyBNF/tree/master/examples/Vax_and_Variants), but we cannot be entirely certain that the samples obtained fully characterize the parameter posteriors of interest. Another concern is that the model incorporates redundant disease-incidence surge mechanisms. In the model, an increase in viral infectiousness caused by the emergence of a new variant can be mimicked, to some extent, by a relaxation of social distancing, and vice versa. For the MSAs considered here, inferred social-distancing levels were low at the time of Alpha and Delta emergence, so the inferred transmissibility factors probably reflect, at least mostly, changes in intrinsic viral infectiousness.

ACKNOWLEDGMENTS

W.S.H., Y.T.L., and A.M. were supported by the LDRD program at Los Alamos National Laboratory (project 20220268ER). Y.C., Z.H., E.F.M., J.N., K.E.N., and R.G.P. were supported by a grant from the National Institute of General Medical Sciences of the National Institutes of Health (grant R01GM111510). A.M. was supported by the 2020 Mathematical Sciences Graduate Internship program, which is sponsored by the Division of Mathematical Sciences of the National Science Foundation, and the Center for Nonlinear Studies at Los Alamos National Laboratory. Computational resources used in this study included Northern Arizona University's Monsoon computer cluster, which is funded by Arizona's Technology and Research Initiative Fund, and the FARM computer cluster at the University of California, Davis. Y.C. thanks Song Chen (University of Wisconsin, La Crosse, Wisconsin, USA) for technical assistance.

REFERENCES

[1] Courtemanche C, Garuccio J, Le A, Pinkston J, Yelowitz A. Strong social distancing measures in the United States reduced the COVID-19 growth rate. Health Aff (Millwood). 2020;39:1237–46. https://doi.org/10.1377/hlthaff.2020.00608

[2] Hsiang S, Allen D, Annan-Phan S, Bell K, Bolliger I, Chong T, et al. The effect of large-scale anti-contagion policies on the COVID-19 pandemic. Nature. 2020;584:262–7. https://doi.org/10.1038/s41586-020-2404-8

[3] Matrajt L, Leung T. Evaluating the effectiveness of social distancing interventions to delay or flatten the epidemic curve of coronavirus disease. Emerg Infect Dis. 2020;26:1740–8. https://doi.org/10.3201/eid2608.201093

[4] Bo Y, Guo C, Lin C, Zeng Y, Li HB, et al. Effectiveness of non-pharmaceutical interventions on COVID-19 transmission in 190 countries from 23 January to 13 April 2020. Int J Inf Dis. 2021;102:247–53. https://doi.org/10.1016/j.ijid.2020.10.066

287 [5] Lin YT, Neumann J, Miller EF, Posner RG, Mallela A, Safta C, Ray J, Thakur G,
288 Chinthavali S, Hlavacek WS. Daily forecasting of regional epidemics of Coronavirus
289 Disease with Bayesian uncertainty quantification, United States. Emerg Infect Dis.
290 2021;27:767–78. https://doi.org/10.3201/eid2703.203364
291 [6] Mallela A, Neumann J, Miller EF, Chen Y, Posner RG, Lin YT, Hlavacek WS. Bayesian
292 inference of state-level COVID-19 basic reproduction numbers across the United States,
293 Viruses. 2022;14:157. https://doi.org/10.3390/v14010157
294 [7] Mallela A, Lin YT, Hlavacek WS. Differential contagiousness of respiratory disease
295 across the United States, medRxiv. 2022. https://doi.org/10.1101/2022.09.15.22279948
296 [8] Oliver SE, Gargano JW, Marin M, Wallace M, Curran KG, Chamberland M, et al. The
297 Advisory Committee on Immunization Practices' interim recommendation for use of
298 Pfizer-BioNTech COVID-19 vaccine—United States, December 2020. MMWR Morb
299 Mortal Wkly Rep. 2020;69:1922–4. https://doi.org/10.15585/mmwr.mm6950e2
300 [9] Oliver SE, Gargano JW, Marin M, Wallace M, Curran KG, Chamberland M, et al. The
301 Advisory Committee on Immunization Practices' interim recommendation for use of
302 Moderna COVID-19 vaccine—United States, December 2020. MMWR Morb Mortal
303 Wkly Rep. 2021;69:1653–6. https://doi.org/10.15585/mmwr.mm695152e1
304 [10] Galloway SE, Paul P, MacCannell DR, Johansson MA, Brooks JT, MacNeil A, et
305 al. Emergence of SARS-CoV-2 B.1.1.7 lineage—United States, December 29, 2020–
306 January 12, 2021. MMWR Morb Mortal Wkly Rep. 2021 / 70(3);95–99.
307 http://dx.doi.org/10.15585/mmwr.mm7003e2
308 [11] Herlihy R, Bamberg W, Burakoff A, Alden N, Severson R, Bush E, et al. Rapid
309 increase in circulation of the SARS-CoV-2 B.1.617.2 (Delta) variant—Mesa County,

Colorado, April–June 2021. MMWR Morb Mortal Wkly Rep. 2021;70:1084–7. https://doi.org/10.15585/mmwr.mm7032e2

[12] Department of Health and Human Services. COVID-19 Vaccine Milestones [cited 2022 Dec 21] https://www.hhs.gov/coronavirus/covid-19-vaccines/distribution/index.html

[13] Daniel W, Nivet M, Warner J, Podolsky DK. Early evidence of the effect of SARS-CoV-2 vaccine at one medical center. N Engl J Med. 2021;384:1962–3. https://doi.org/10.1056/NEJMc2102153

[14] Centers for Disease Control and Prevention. COVID data tracker. 2021 [cited 2021 Oct 6] https://covid.cdc.gov/covid-data-tracker/#datatracker-home

[15] Coronavirus Resource Center, Johns Hopkins University. Impact of opening and closing decisions by state: a look at how social distancing measures may have influenced trends in COVID-19 cases and deaths. 2021 [cited 2021 Oct 6] https://coronavirus.jhu.edu/data/state-timeline

[16] Washington NL, Gangavarapu K, Zeller M, Bolze A, Cirulli ET, Schiabor Barrett KM, et al. Emergence and rapid transmission of SARS-CoV-2 B.1.1.7 in the United States. Cell. 2021;184:2587–94. https://doi.org/10.1016/j.cell.2021.03.052

[17] Centers for Disease Control and Prevention. Covid data tracker, variant proportions. 2021 [cited 2021 Oct 6] https://covid.cdc.gov/covid-data-tracker/#variant-proportions

[18] Volz E, Mishra S, Chand M, Barrett JC, Johnson R, Geidelberg L, et al. Assessing transmissibility of SARS-CoV-2 lineage B.1.1.7 in England. Nature. 2021;593:266–9. https://doi.org/10.1038/s41586-021-03470-x

[19] Davies NG, Abbott S, Barnard RC, Jarvis CI, Kucharski AJ, Munday JD, et al. Estimated transmissibility and impact of SARS-CoV-2 lineage B.1.1.7 in England. Science. 2021;372:eabg3055. https://doi.org/10.1126/science.abg3055

[20] Ito K, Piantham C, Nishiura H. Predicted dominance of variant Delta of SARS-CoV-2 before Tokyo Olympic Games, Japan, July 2021. Euro Surveill. 2021;26:2100570. https://doi.org/10.2807/1560-7917.ES.2021.26.27.2100570

[21] Arav Y, Fattal E, Klausner Z. Increased transmissibility of emerging SARS-CoV-2 variants is driven either by viral load or probability of infection rather than environmental stability. Mathematics. 2022, 10(19), 3422. https://doi.org/10.3390/math10193422

[22] Public Health England. SARS-CoV-2 variants of concern and variants under investigation in England. Technical briefing 15, June 11, 2021. [cited 2021 Aug 24] https://assets.publishing.service.gov.uk/government/uploads/system/uploads/attachment_data/file/993879/Variants_of_Concern_VOC_Technical_Briefing_15.pdf

[23] Cascella M, Rajnik M, Aleem A, Dulebohn SC, Di Napoli R. Features, evaluation, and treatment of coronavirus (COVID-19). July 30, 2021 update. Treasure Island (FL): StatPearls Publishing; 2022. https://www.ncbi.nlm.nih.gov/books/NBK554776/

[24] Lopez Bernal J, Andrews N, Gower C, Gallagher E, Simmons R, Thelwall S, et al. Effectiveness of Covid-19 Vaccines against the B.1.617.2 (Delta) variant. N Engl J Med. 2021;385:585–94. https://doi.org/10.1056/NEJMoa2108891

[25] Rovida F, Cassaniti I, Paolucci S, Percivalle E, Sarasini A, Piralla A, et al. SARS-CoV-2 vaccine breakthrough infections with the alpha variant are asymptomatic or

356 mildly symptomatic among health care workers. Nat Commun. 2021;12:6032.
357 https://doi.org/10.1038/s41467-021-26154-6
358 [26] The New York Times. Coronavirus (Covid-19) data in the United States. 2021
359 [cited 2021 Aug 24] https://github.com/nytimes/covid-19-data
360 [27] Covid Act Now. US COVID risk and vaccine tracker. 2021 [cited 2021 Sep 29]
361 https://covidactnow.org/
362 [28] Neumann J, Lin YT, Mallela A, Miller EF, Colvin J, Duprat AT, Chen Y,
363 Hlavacek WS, Posner RG. Implementation of a practical Markov chain Monte Carlo
364 sampling algorithm in PyBioNetFit. Bioinformatics. 2022;38:1770–2.
365 https://doi.org/10.1093/bioinformatics/btac004
366 [29] Vats D, Knudson C. Revisiting the Gelman-Rubin Diagnostic. Statist. Sci.
367 2021;36:518–529. https://doi.org/10.1214/20-STS812
368 [30] Centers for Disease Control and Prevention. SARS-CoV-2 Variant Proportions.
369 2023 [cited 2023 Mar 8] https://data.cdc.gov/Laboratory-Surveillance/SARS-CoV-2-
370 Variant-Proportions/jr58-6ysp

371

372 **Table 1.** Model parameter values inferred for the Dallas, Houston, New York City, and Phoenix

373 Metropolitan Statistical Areas (MSAs) on October 31, 2021

Parameter	MAP estimate* for Dallas (Units)	MAP estimate* for Houston (Units)	MAP estimate* for New York City (Units)	MAP estimate* for Phoenix (Units)
t_0	12.0 (d)	11.7 (d)	8.6 (d)	15.0 (d)
β	0.29 (d^{-1})	0.29 (d^{-1})	0.37 (d^{-1})	0.28 (d^{-1})
σ	57 (d)	58 (d)	60 (d)	56 (d)
p_0	0.31	0.32	0.48	0.32
λ_0	6.8 (d^{-1})	6.8 (d^{-1})	10.0 (d^{-1})	8.5 (d^{-1})
τ_1	62 (d)	61 (d)	64 (d)	40 (d)
p_1	0.26	0.26	0.41	0.20
λ_1	2.2 (d^{-1})	2.4 (d^{-1})	3.1 (d^{-1})	1.5 (d^{-1})
τ_2	46 (d)	52 (d)	29 (d)	51 (d)
p_2	0.34	0.32	0.42	0.36
λ_2	2.0 (d^{-1})	2.8 (d^{-1})	0.34 (d^{-1})	3.1 (d^{-1})
τ_3	83 (d)	99 (d)	76 (d)	79 (d)
p_3	0.19	0.18	0.30	0.19
λ_3	2.4 (d^{-1})	2.5 (d^{-1})	8.3 (d^{-1})	1.6 (d^{-1})
τ_4	131 (d)	-	-	213 (d)
p_4	0.10	-	-	0.19
λ_4	1.6 (d^{-1})	-	-	2.0 (d^{-1})

θ_1	427 (d)	434 (d)	392 (d)	437 (d)
y_1	1.1	1.2	1.3	1.6
θ_2	92 (d)	83 (d)	120 (d)	80 (d)
y_2	1.6	1.8	2.2	2.2
f_D	0.37	0.32	0.39	0.53
r	3.2	2.8	9.4	3.4

*Maximum *a posteriori* (MAP) estimates are region-specific and inference-time-dependent. Here, inference was based on MSA-specific confirmed coronavirus disease case count data available in the GitHub repository maintained by *The New York Times* newspaper [26] for January 21, 2020 to October 31, 2021. Time $t = 0$ corresponds to midnight on January 21, 2020. Inferences were conditioned on the compartmental model of Appendix Equations 1–38, consideration of two viral variants (Alpha and Delta, $m = 2$), and $n + 1$ distinct social-distancing periods in total ($n = 4$ for Dallas and Phoenix; $n = 3$ for New York City and Houston), the fixed parameter estimates of Table 3, and the initial condition I_0 and S_0 at time $t = t_0$ given in Table 3. The choice of two variants and the setting for n were chosen through a model-selection procedure described in the Appendix. With $m = 2$ and $n = 3$, there are 18 adjustable model parameters: t_0, β, θ_1, y_1, θ_2, y_2, σ, p_0, λ_0, τ_1, p_1, λ_1, τ_2, p_2, λ_2, τ_3, p_3, and λ_3. With $m = 2$ and $n = 4$, there are 21 adjustable model parameters: t_0, β, θ_1, y_1, θ_2, y_2, σ, p_0, λ_0, τ_1, p_1, λ_1, τ_2, p_2, λ_2, τ_3, p_3, λ_3, τ_4, p_4, and λ_4. These parameters were jointly inferred together with f_D, the parameter of the measurement model (i.e., the fraction of new cases detected and reported) (Appendix Equation 40), and r, the dispersion parameter of the statistical model for noise in case detection and reporting (i.e., the adjustable parameter of the negative binomial

likelihood function) (Appendix Equations 41–43). We assumed a uniform proper prior, as described in the Appendix.

394 **Table 2.** Descriptions of MSA-specific adjustable model parameters.

Parameter	Description
t_0	Start of local disease transmission
β	Rate constant for disease transmission
σ	Start of first social-distancing period
p_0	Social-distancing setpoint for the period $t \in [\sigma, \tau_1)$
λ_0	Social-distancing eigenvalue paired with p_0
τ_1	Start of second social-distancing period
p_1	Social-distancing setpoint for the period $t \in [\tau_1, \tau_2)$
λ_1	Social-distancing eigenvalue paired with p_1
τ_2	Start of third social-distancing period
p_2	Social-distancing setpoint for the period $t \in [\tau_2, \tau_3)$
λ_2	Social-distancing eigenvalue paired with p_2
τ_3	Start of fourth social-distancing period
p_3	Social-distancing setpoint for the period $t \in [\tau_3, \tau_4)$
λ_3	Social-distancing eigenvalue paired with p_3
τ_4	Start of fifth social-distancing period
p_4	Social-distancing setpoint for the period $t \in [\tau_4, \infty)$
λ_4	Social-distancing eigenvalue paired with p_4
θ_1	Alpha takeoff time
y_1	Increased infectiousness of Alpha (relative to ancestral strains)

θ_2	Delta takeoff time
y_2	Increased infectiousness of Delta (relative to ancestral strains)
f_D	Fraction of cases detected and reported
r	Dispersion parameter of NB(r, q_i)*

*The probability parameter of NB(r, q_i) is constrained, i.e., the value of q_i, which is reporting time-dependent, is given by Appendix Equation 43.

413 **Table 3.** Fixed parameter estimates for each region-specific compartmental model

Parameter	Estimate[1] (Units)	Description	Source
I_0	1	Number of infectious persons at time $t = t_0$	[5]
S_0	19,216,182[2]	Total population	[5]
$\mu(t)$	Empirical time-series[3] (d^{-1})	Daily *per capita* rate of vaccination	[27]
m_b	0.1	Reduction in risk of infection because of social distancing	[5]
m_h	0.04	Reduction in risk of severe disease (once symptomatic) because of vaccination	This study[4]
f_A	0.44	Fraction of all cases that are asymptomatic	[5]
f_H	0.054	Fraction of symptomatic cases that are severe (in the absence of vaccination)	[5]
f_R	0.79	Fraction of persons with severe disease who recover	[5]
$1 - f_0$	0.1	Fraction of vaccinated persons who fail to develop an immune response that protects against productive infection by ancestral strains or variants	This study[4]
$f_0 - f_1$	0.09	Fraction of vaccinated persons who develop an immune response that protects against	This study[4]

		productive infection by ancestral strains (but not the Alpha or Delta variant)	
$f_1 - f_2$	0.12	Fraction of vaccinated persons who develop an immune response that protects against productive infection by ancestral strains and the Alpha variant (but not the Delta variant)	This study[4]
f_2	0.69	Fraction of vaccinated persons who develop an immune response that protects against productive infection by ancestral strains and the Alpha and Delta variants	This study[4]
ρ_E	1.1	Relative infectiousness of persons without symptoms in the incubation period of infection	[5]
ρ_A	0.9	Relative infectiousness of persons without symptoms in the immune-clearance phase of infection	[5]
k_L	0.94 (d^{-1})	Rate constant for progression through each stage of the incubation period of infection[5]	[5]
k_Q	0.0038 (d^{-1})	Rate constant for quarantine of infected, non-vaccinated persons	[5]
j_Q	0.4 (d^{-1})	Rate constant for self-isolation of symptomatic, non-vaccinated persons	[5]

c_A	0.26 (d^{-1})	Rate constant for completion of the immune clearance phase of infection for persons without symptoms	[5]
c_I	0.12 (d^{-1})	Rate constant for completion of the immune clearance phase of infection or progression to severe disease for non-vaccinated persons with symptoms	[5]
c_H	0.17 (d^{-1})	Rate constant for recovery or progression to death for non-vaccinated persons with severe disease	[5]
k_V	0.3 (d^{-1})	Rate constant for progression through each stage of immune response to vaccination[6]	This study[4]

[1]Fixed parameter estimates are based on information external to the surveillance data used to infer the adjustable parameter values of Table 1. Estimates are applicable to all metropolitan statistical areas (MSAs) of interest except for S_0 and the vaccination function $\mu(t)$, which are region-specific. Recall that $\mu(t)$ is updated daily for consistency with vaccination data.

[2]The total population S_0 is MSA-specific. Here, S_0 is given for the New York City MSA. The initial susceptible population is taken to be the total population. We used $S_0 = 7{,}573{,}136$, 7,066,141, and 4,873,019 for the Dallas, Houston, and Phoenix MSAs, respectively.

[3]The function $\mu(t)$ is determined by region-specific vaccination data [27].

[4]See the Appendix for more information about estimates of fixed parameter values made in this study.

[5]As in the study of Lin et al. [5], the incubation period is divided into 5 stages (Figure 1), each of equal duration on average.

[6]The immune response to vaccination is divided into 6 stages (Figure 1), each of equal duration on average. The choice of 6 stages is justified in the Appendix and Appendix Figure 2.

Table 4. Multivariate potential scale reduction factors (PSRFs) and multivariate effective sample sizes (ESSs) corresponding to the stable Gelman-Rubin statistic for Markov chains generated using PyBioNetFit for the Dallas, Houston, New York City, and Phoenix Metropolitan Statistical Areas (MSAs)

MSA	Multivariate PSRF[1]	Multivariate ESS[1]
Dallas	1.0016	317.2
Houston	1.0021	239.9
New York City	1.0022	225.9
Phoenix	1.0034	146.2

[1]Computed using the methodology of Vats and Knudson [29].

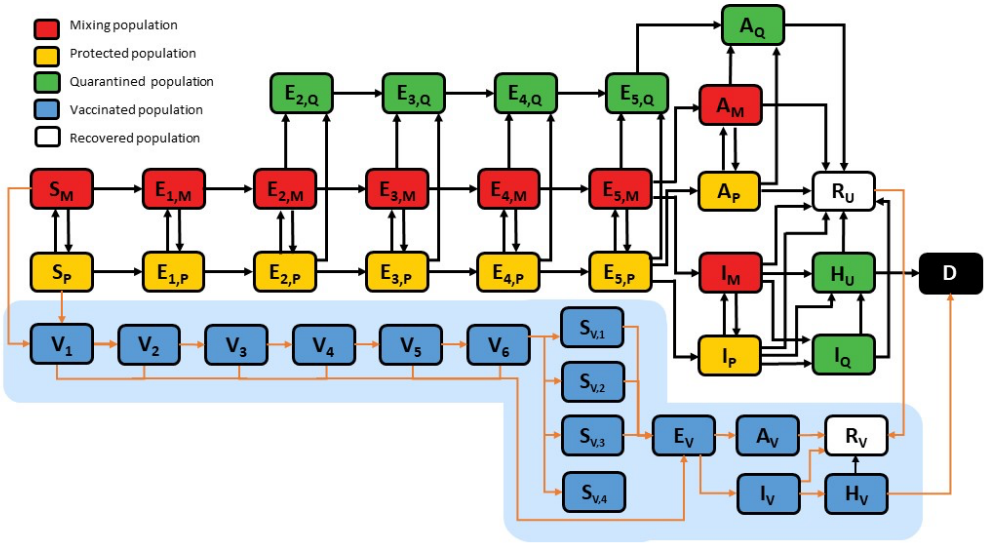

438

439 **Figure 1.** Illustration of compartmental model. The independent variable of the model is time t.
440 The 40 dependent state variables of the model are populations, which are represented as boxes
441 with rounded corners. A description of each state variable is given in Appendix Table 1. The 15
442 highlighted boxes (on the blue background) represent state variables introduced to capture the
443 effects of vaccination and the Alpha and Delta variants. The other 25 boxes represent state
444 variables considered in the model of Lin et al. [5]. Arrows connecting boxes represent
445 transitions. Each transition represents the movement of persons from one population to another.
446 The arrows highlighted in orange represent transitions introduced to capture the effects of
447 vaccination and the Alpha and Delta variants. Other arrows represent transitions considered in
448 the model of Lin et al. [5]. Each arrow is associated with one or more parameters that
449 characterize a rate of movement; these parameters are not shown here but are shown in Appendix
450 Figure 1. A full description of the model is given in the Appendix. Briefly, new parts of the
451 model can be described as follows. Vaccination is modeled by moving susceptible persons (in

452 the S_M and S_P populations) into the V_1 population. Another consequence of vaccination is the
453 movement of recovered unvaccinated persons (in the R_U population) into the R_V population. The
454 rate of vaccination typically changes from day to day to match the empirical daily rate of
455 vaccination. Recovered and susceptible persons have the same *per-capita* probability of
456 vaccination. Persons in S_M are mixing (i.e., not practicing social distancing) and persons in S_P
457 are practicing social distancing (and thereby protected from infection to a degree). The series of
458 transitions involving the populations $V_1, \ldots, V_6$ was introduced to model the immune response to
459 vaccination (i.e., the amount of time required for vaccination to induce neutralizing antibodies).
460 With this approach, the time from vaccination to appearance of neutralizing antibodies is a
461 random variable characterized by an Erlang distribution. Persons in $V_1, \ldots, V_6$ may be infected.
462 Persons in V_6 transition to one of the following four populations: $S_{V,1}, \ldots, S_{V,4}$. These populations
463 represent persons with varying degrees of immune protection. Persons in $S_{V,1}$ are not protected
464 against productive infection (i.e., an infection that can be transmitted to others) by any viral
465 strain. Persons in $S_{V,2}$ are protected against productive infection by viral strains present before
466 the emergence of Alpha but not Alpha or Delta. Persons in $S_{V,3}$ are protected against productive
467 infection by viral strains present before the emergence of Alpha and also Alpha but not Delta.
468 Persons in $S_{V,4}$ are protected against productive infection by all of the viral strains considered up
469 to October 31, 2021. Vaccinated persons who become infected move into E_V. The time spent in
470 E_V corresponds to the length of the incubation period for vaccinated persons. The mean duration
471 of the incubation period is taken to be the same for vaccinated and unvaccinated persons;
472 however, as a simplification, for vaccinated persons, the time spent in the incubation period is
473 taken to consist of a single stage and consequently is exponentially distributed (vs. Erlang
474 distributed for unvaccinated persons). All non-quarantined exposed persons (in populations E_V

475 and $E_{i,M}$ and $E_{i,P}$ for $i = 1, \ldots, 5$) are taken to be infectious. Persons exiting E_V leave the
476 incubation period and enter the immune clearance phase of infection, during which they may be
477 asymptomatic (A_V) or symptomatic with mild disease (I_V). All non-quarantined asymptomatic
478 persons (in populations A_V, A_M, and A_P) are taken to be infectious. Persons in A_V are all assumed
479 to eventually recover (i.e., to enter R_V). Persons with mild symptomatic disease may recover
480 (i.e., enter R_V) or experience severe disease, at which point they move to H_V (in hospital or
481 isolated at home). Vaccinated persons have a diminished probability of severe disease in
482 comparison to unvaccinated persons. Persons in H_V either recover (move to R_V) or die from
483 COVID-19 complications (move to D). For a person with severe disease, the probability of death
484 is independent of vaccination status. We assume that vaccinated persons do not participate in
485 social distancing, quarantine, or self-isolation driven by symptom awareness.

486
487

A

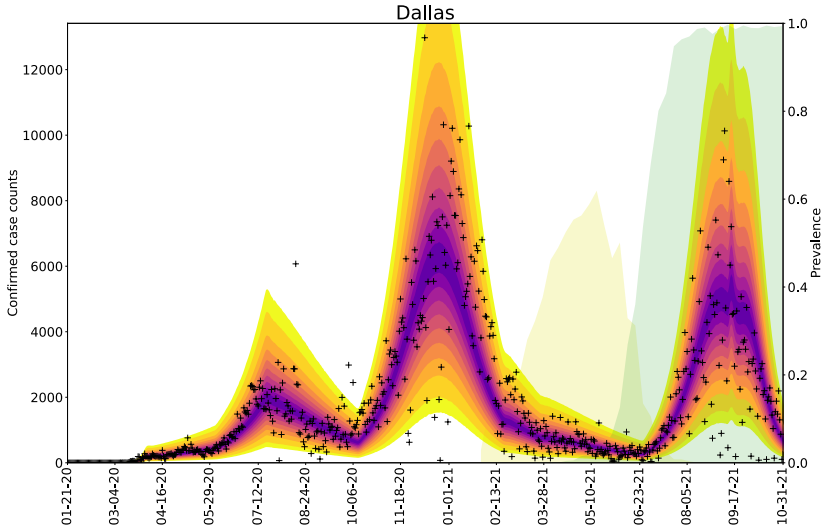

B

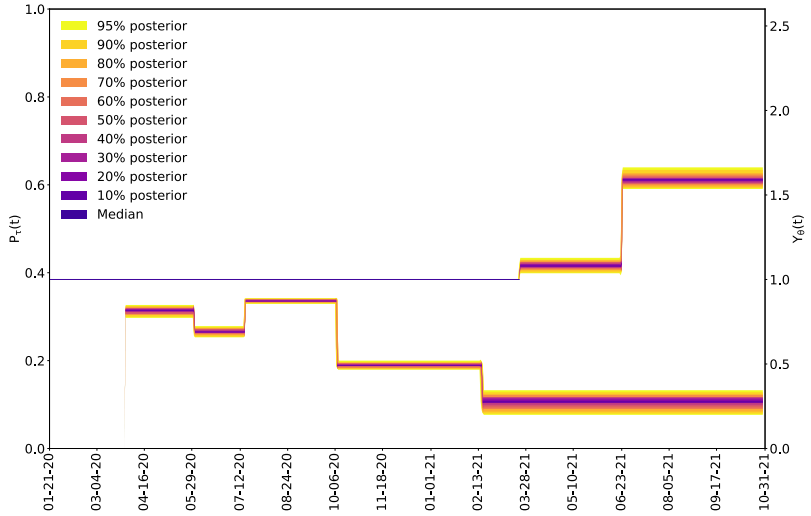

C

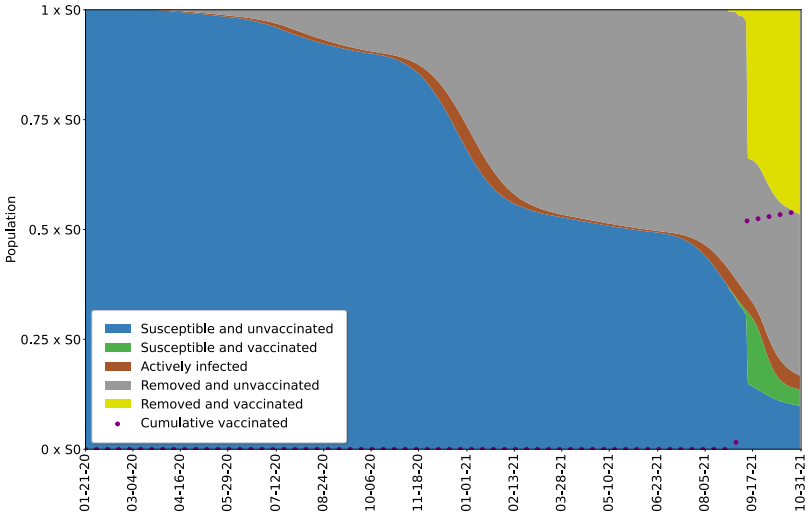

Figure 2. Inference results obtained for the MSA surrounding Dallas using regional surveillance data—daily reports of new COVID-19 cases—available for January 21, 2020 to October 31, 2021. A) Credible intervals of the time-dependent posterior predictive distribution for detected and reported new cases are shown. The color bands from bottom to top indicate the 5%, 10%, … 90%, 95% credible intervals. This colored region all together indicates the 95% credible interval and can be expected to cover approximately 95% of the data. Empirical case reports are indicated by black symbols. A case count of 12,974 cases on December 11, 2020 is not shown in the plot. Alpha prevalence is indicated with a shaded light-yellow background. Delta prevalence is indicated with a shaded light-green background. B) The social-distancing stationary setpoint is given by $P_\tau(t)$ and the variant transmissibility factor is given by $Y_\theta(t)$. Note that the values of $P_\tau(t)$ and $Y_\theta(t)$ are dimensionless. Credible intervals corresponding to 1000 samples from the time-dependent posterior predictive distributions are shown for $P_\tau(t)$ and $Y_\theta(t)$. The curve corresponding to $Y_\theta(t)$ is monotonically increasing with an initial value of 1. The curve corresponding to $P_\tau(t)$ is decreasing from left to right after the start of social distancing. C) Inferred changes in the distribution of persons amongst five selected subpopulations over the course of the local COVID-19 epidemic. The five populations sum to a constant, S_0, the total population. Results shown here are based on the parameter values given in Tables 1 and 3. The five populations are defined as follows: the population of susceptible unvaccinated persons (blue area) is given by $S_M + S_P$, the population of susceptible vaccinated persons (green area) is given by $\sum_{i=1}^{6} V_i + S_{V,1} + U_{\theta_1}(t)S_{V,2} + U_{\theta_2}(t)S_{V,3}$, the population of actively infected persons (orange area) is given by $H_U + H_V + E_V + \sum_{i=1}^{5}\left(E_{i,M} + E_{i,P} + E_{i,Q}\right) + \sum_{x\in\{M,P,Q,V\}}(A_x + I_x)$, the population of removed unvaccinated persons (gray area) is given by $R_U + D$, and the population of removed vaccinated persons (yellow area) is given by $R_V + (1 - U_{\theta_1}(t))S_{V,2} +$

512 $(1 - U_{\theta_2}(t))S_{V,3} + S_{V,4}$. Except for $U_{\theta_1}(t)$ and $U_{\theta_2}(t)$, the terms in the above definitions refer to
513 state variables of the compartmental model of Figure 1 and Appendix Figure 1, which are
514 defined in Appendix Table 1. $U_{\theta_1}(t)$ and $U_{\theta_2}(t)$ are unit step functions (Appendix Equation 33
515 and 34), which change value from 0 to 1 at time $t = \theta_1$ and $t = \theta_2$, respectively. Recall that θ_1
516 and θ_2 are the Alpha and Delta takeoff times. The sum $\sum_i(\mu_i \times 1\text{ d})$ (purple dots), which is the
517 empirical cumulative number of completed vaccinations, is shown as a function of time t.
518

A

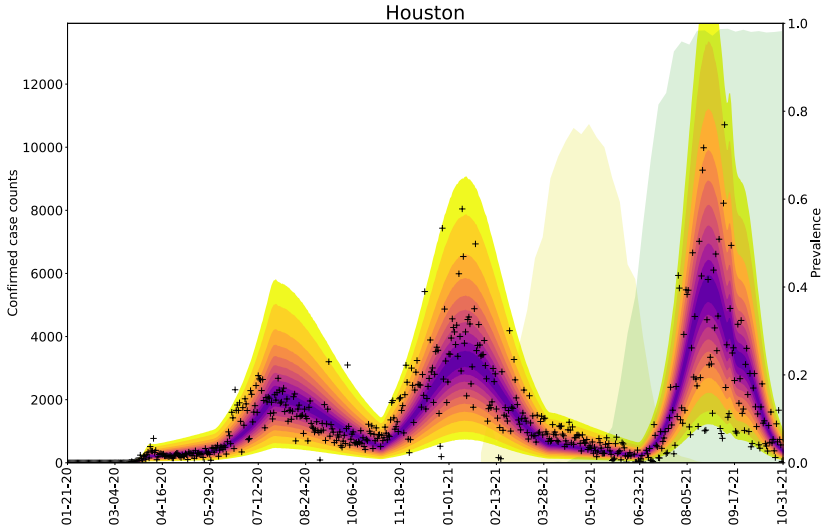

B

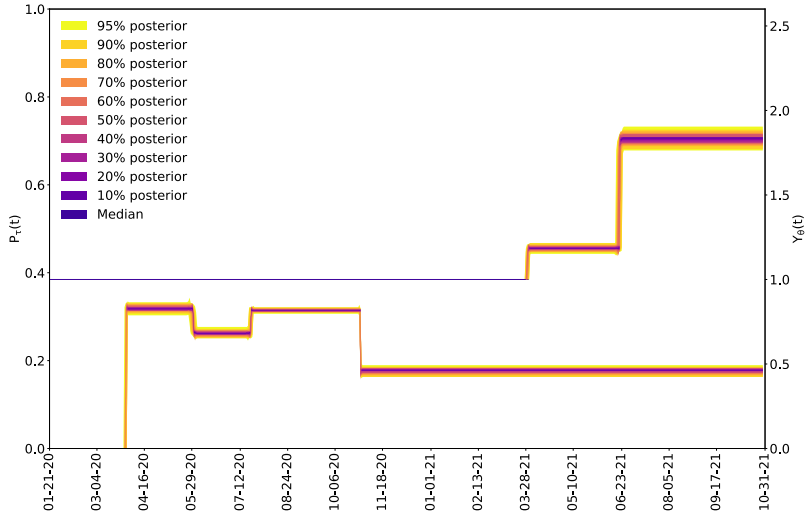

C

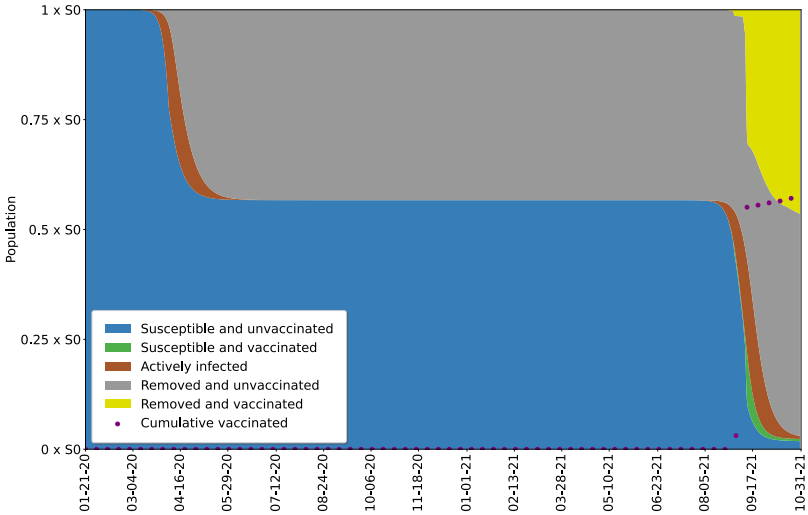

520 **Figure 3.** Inference results obtained for the MSA surrounding Houston using regional
521 surveillance data—daily reports of new COVID-19 cases—available for January 21, 2020 to
522 October 31, 2021. It should be noted that four anomalous (negative) empirical case counts are
523 not shown in the plot. A case count of 14,300 cases on September 21, 2020 is not shown in the
524 plot. See the caption of Figure 2 for additional information.

525

A

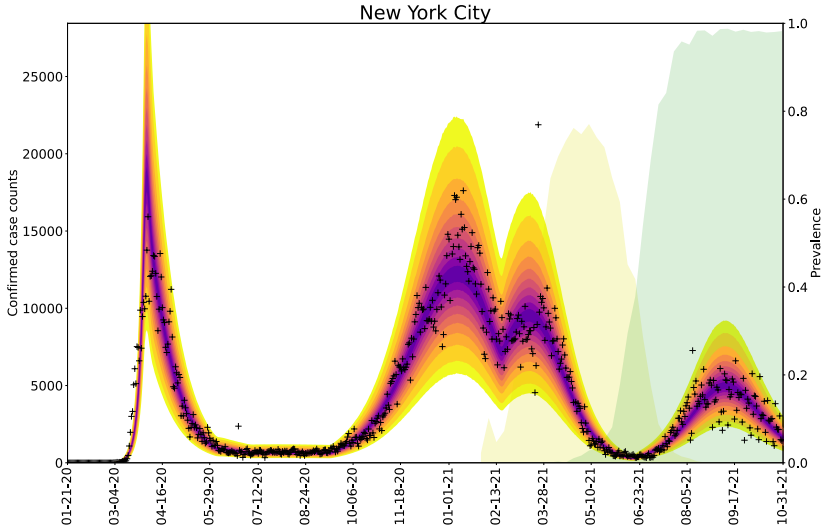

B

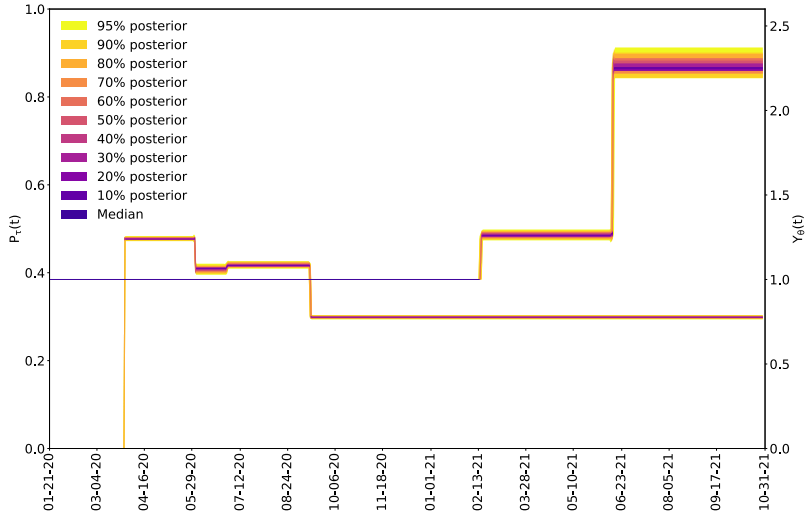

C

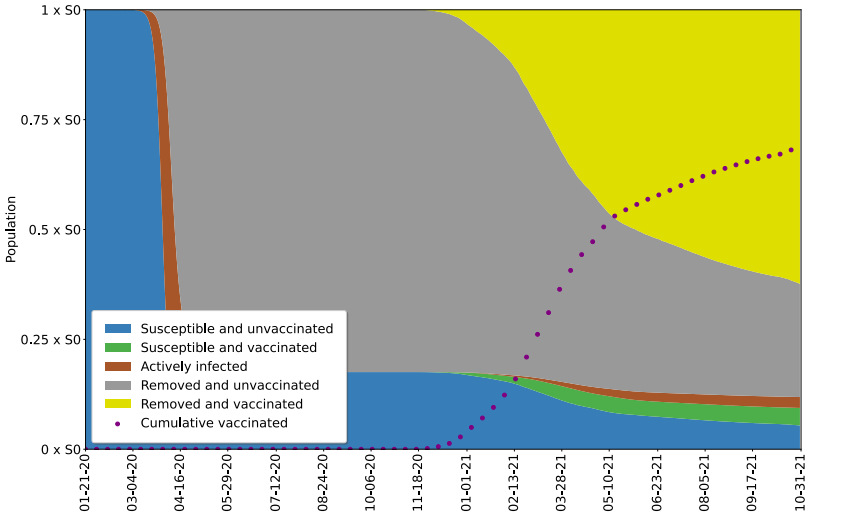

Figure 4. Inference results obtained for the MSA surrounding New York City using regional surveillance data—daily reports of new COVID-19 cases—available for January 21, 2020 to October 31, 2021. It should be noted that a single anomalous (negative) empirical case count is not shown in the plot. A case count of 42,774 cases on January 3, 2021 is not shown in the plot. See the caption of Figure 2 for additional information.

A

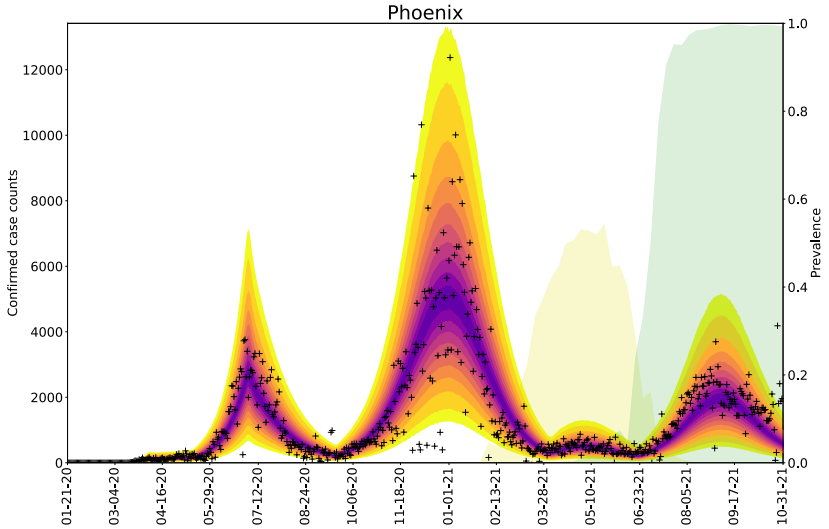

B

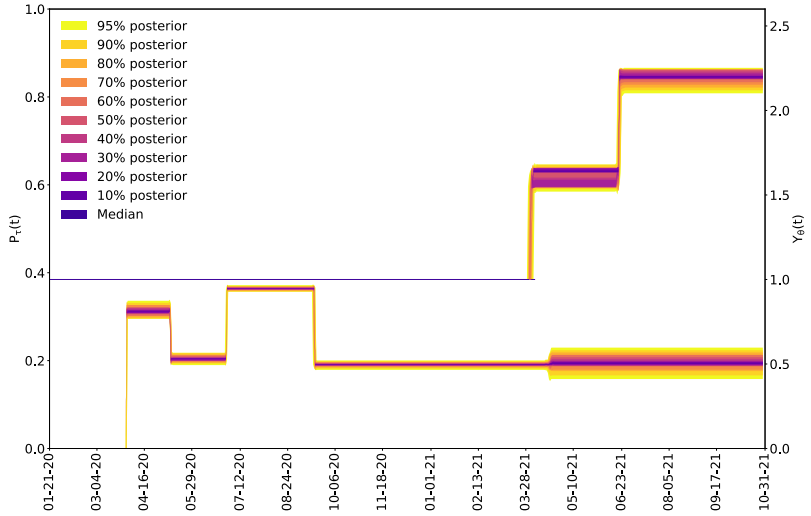

C

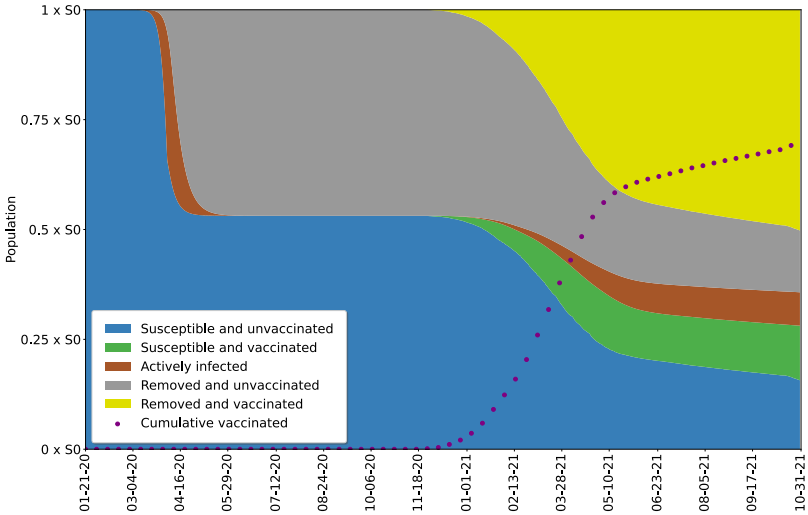

542 **Figure 5.** Inference results obtained for the MSA surrounding Phoenix using regional
543 surveillance data—daily reports of new COVID-19 cases—available for January 21, 2020 to
544 October 31, 2021. It should be noted that two anomalous (negative) empirical case counts are not
545 shown in the plot. A case count of 12,372 cases on January 3, 2021 is not shown in the plot. See
546 the caption of Figure 2 for additional information.
547
548
549
550
551
552
553
554
555
556
557

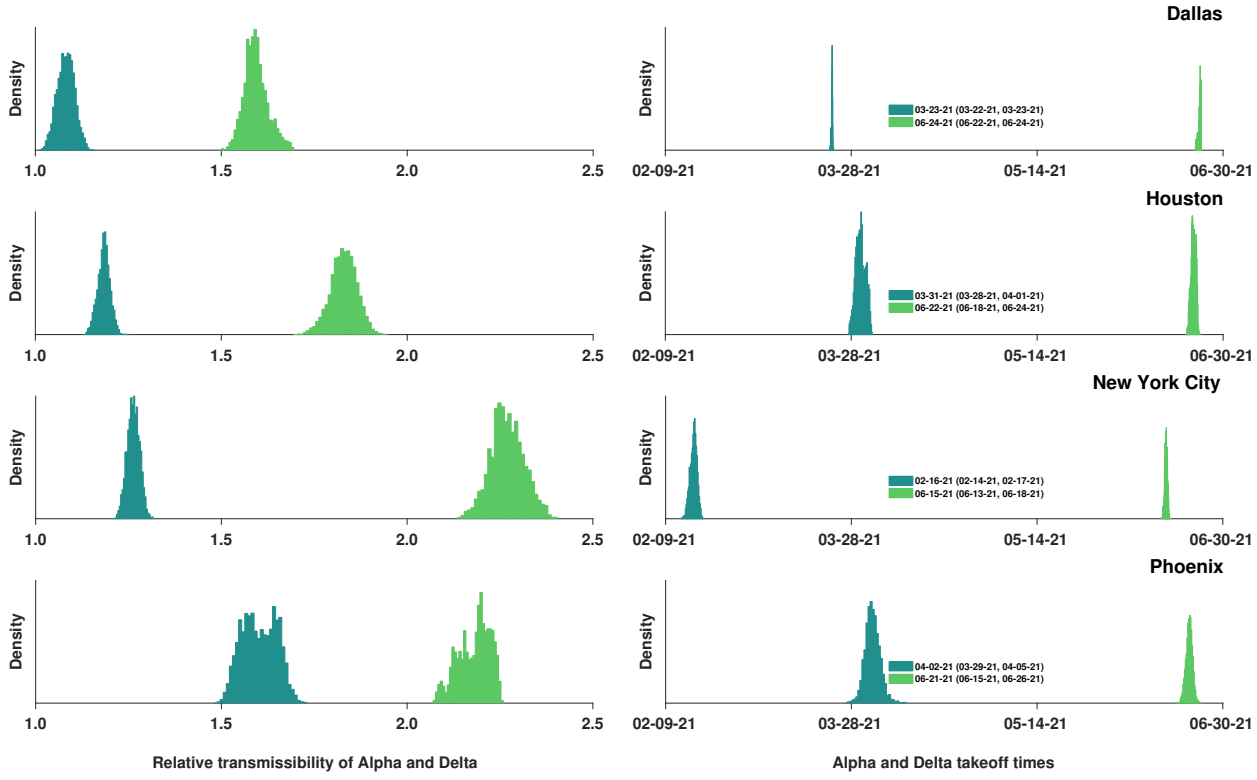

Figure 6. Marginal posterior distributions of transmissibility factors for Alpha in dark-green and Delta in light-green (left panels) and takeoff times for Alpha and Delta (right panels) in four MSAs centered on (**A**,**B**) Dallas, (**C**,**D**) Houston, (**E**,**F**) New York City, and (**G**,**H**) Phoenix. Inferences are based on daily reports of new cases from January 21, 2020 to October 31, 2021. For each of the right panels, the 95% credible intervals for Alpha and Delta takeoff times are indicated in parentheses, and the MAP estimate for a given region is indicated to the left of the credible interval.

APPENDIX

Imputation of Missing Daily Case Counts

By October 31, 2021, many regions in the US were not reporting new detected COVID-19 cases on a strictly daily basis. When one or more daily case counts were not available, we imputed daily case counts on the basis of a linear fit to the two nearest available cumulative case counts. This approach has the effect of evenly distributing case counts across the days for which daily reports are unavailable.

Equations of the Compartmental Model

The compartmental model, which is illustrated in Figure 1 and Appendix Figure 1, consists of the following 40 ordinary differential equations (ODEs):

$$\frac{dS_M}{dt} = -\beta Y_\theta(t)\left(\frac{S_M}{S_0}\right)\left(\phi_M(t,\rho) + m_b\phi_P(t,\rho)\right) - U_\sigma(t)\Lambda_\tau(t)\left[P_\tau(t)S_M - \left(1-P_\tau(t)\right)S_P\right] - \mu(t)S_0\left(\frac{S_M}{\phi_V(t)}\right) \quad (1)$$

$$\frac{dS_P}{dt} = -m_b\beta Y_\theta(t)\left(\frac{S_P}{S_0}\right)\left(\phi_M(t,\rho) + m_b\phi_P(t,\rho)\right) + U_\sigma(t)\Lambda_\tau(t)\left[P_\tau(t)S_M - \left(1-P_\tau(t)\right)S_P\right] - \mu(t)S_0\left(\frac{S_P}{\phi_V(t)}\right) \quad (2)$$

$$\frac{dE_{1,M}}{dt} = \beta Y_\theta(t)\left(\frac{S_M}{S_0}\right)\left(\phi_M(t,\rho) + m_b\phi_P(t,\rho)\right) - k_L E_{1,M} - U_\sigma(t)\Lambda_\tau(t)\left[P_\tau(t)E_{1,M} - (1-P_\tau(t))E_{1,P}\right] \quad (3)$$

$$\frac{dE_{1,P}}{dt} = m_b\beta Y_\theta(t)\left(\frac{S_P}{S_0}\right)(\phi_M(t,\rho) + m_b\phi_P(t,\rho)) - k_L E_{1,P} + U_\sigma(t)\Lambda_\tau(t)\left[P_\tau(t)E_{1,M} - (1-P_\tau(t))E_{1,P}\right] \quad (4)$$

$$\frac{dE_{i,M}}{dt} = k_L E_{i-1,M} - k_L E_{i,M} - k_Q E_{i,M} - U_\sigma(t)\Lambda_\tau(t)\left[P_\tau(t)E_{i,M} - (1-P_\tau(t))E_{i,P}\right], \quad (5)$$

for $i = 2, 3, 4, 5$

$$\frac{dE_{i,P}}{dt} = k_L E_{i-1,P} - k_L E_{i,P} - k_Q E_{i,P} + U_\sigma(t)\Lambda_\tau(t)\left[P_\tau(t)E_{i,M} - (1-P_\tau(t))E_{i,P}\right], \quad (6)$$

for $i = 2, 3, 4, 5$

$$\frac{dE_{2,Q}}{dt} = k_Q(E_{2,M} + E_{2,P}) - k_L E_{2,Q} \quad (7)$$

$$\frac{dE_{i,Q}}{dt} = k_Q\left(E_{i,M} + E_{i,P}\right) + k_L E_{i-1,Q} - k_L E_{i,Q}, \text{ for } i = 3, 4, 5 \quad (8)$$

$$\frac{dA_M}{dt} = f_A k_L E_{5,M} - k_Q A_M - U_\sigma(t)\Lambda_\tau(t)[P_\tau(t)A_M - (1-P_\tau(t))A_P] - c_A A_M \quad (9)$$

$$\frac{dA_P}{dt} = f_A k_L E_{5,P} - k_Q A_P + U_\sigma(t)\Lambda_\tau(t)[P_\tau(t)A_M - (1-P_\tau(t))A_P] - c_A A_P \quad (10)$$

$$\frac{dA_Q}{dt} = f_A k_L E_{5,Q} + k_Q(A_M + A_P) - c_A A_Q \quad (11)$$

$$\frac{dI_M}{dt} = (1-f_A)k_L E_{5,M} - \left(k_Q + j_Q\right)I_M - U_\sigma(t)\Lambda_\tau(t)\left[P_\tau(t)I_M - \left(1-P_\tau(t)\right)I_P\right] - c_I I_M \quad (12)$$

$$\frac{dI_P}{dt} = (1-f_A)k_L E_{5,P} - \left(k_Q + j_Q\right)I_P + U_\sigma(t)\Lambda_\tau(t)[P_\tau(t)I_M - \left(1-P_\tau(t)\right)I_P] - c_I I_P \quad (13)$$

$$\frac{dI_Q}{dt} = (1 - f_A)k_L E_{5,Q} + \left(k_Q + j_Q\right)(I_M + I_P) - c_I I_Q \tag{14}$$

$$\frac{dH_U}{dt} = f_H c_I\left(I_M + I_P + I_Q\right) - c_H H_U \tag{15}$$

$$\frac{dD}{dt} = (1 - f_R)c_H H_U + (1 - f_R)c_H H_V \tag{16}$$

$$\frac{dR_U}{dt} = c_A\left(A_M + A_P + A_Q\right) + (1 - f_H)c_I\left(I_M + I_P + I_Q\right) + f_R c_H H_U - \mu(t)S_0\left(\frac{R_U}{\phi_V(t)}\right) \tag{17}$$

$$\frac{dV_1}{dt} = \mu(t)S_0\left(\frac{S_M + S_P}{\phi_V(t)}\right) - k_V V_1 - \beta Y_\theta(t)\left(\frac{V_1}{S_0}\right)\left(\phi_M(t,\rho) + m_b\phi_P(t,\rho)\right) \tag{18}$$

$$\frac{dV_i}{dt} = k_V V_{i-1} - k_V V_i - \beta Y_\theta(t)\left(\frac{V_i}{S_0}\right)\left(\phi_M(t,\rho) + m_b\phi_P(t,\rho)\right), \tag{19}$$

$$\text{for } i = 2, 3, 4, 5, 6$$

$$\frac{dS_{V,1}}{dt} = (1 - f_0)k_V V_6 - \beta Y_\theta(t)\left(\frac{S_{V,1}}{S_0}\right)\left(\phi_M(t,\rho) + m_b\phi_P(t,\rho)\right) \tag{20}$$

$$\frac{dS_{V,2}}{dt} = (f_0 - f_1)k_V V_6 - U_{\theta_1}(t)\beta Y_\theta(t)\left(\frac{S_{V,2}}{S_0}\right)\left(\phi_M(t,\rho) + m_b\phi_P(t,\rho)\right) \tag{21}$$

$$\frac{dS_{V,3}}{dt} = (f_1 - f_2)k_V V_6 - U_{\theta_2}(t)\beta Y_\theta(t)\left(\frac{S_{V,3}}{S_0}\right)\left(\phi_M(t,\rho) + m_b\phi_P(t,\rho)\right) \tag{22}$$

$$\frac{dS_{V,4}}{dt} = f_2 k_V V_6 \tag{23}$$

$$\frac{dE_V}{dt} = \beta Y_\theta(t)\left(\frac{1}{S_0}\right)\left(\phi_M(t,\rho) + m_b\phi_P(t,\rho)\right) \cdot \sum_{i=1}^{6}\left(V_i + S_{V,1} + U_{\theta_1}(t)S_{V,2} + U_{\theta_2}(t)S_{V,3}\right) - \left(\frac{k_L}{5}\right)E_V \tag{24}$$

$$\frac{dA_V}{dt} = f_A\left(\frac{k_L}{5}\right)E_V - c_A A_V \tag{25}$$

$$\frac{dI_V}{dt} = (1 - f_A)\left(\frac{k_L}{5}\right)E_V - c_I I_V \tag{26}$$

$$\frac{dH_V}{dt} = m_h f_H c_I I_V - c_H H_V \tag{27}$$

$$\frac{dR_V}{dt} = \mu(t)S_0\left(\frac{R_U}{\phi_V(t)}\right) + c_A A_V + (1 - m_h f_H)c_I I_V + f_R c_H H_V \tag{28}$$

In these equations, the independent variable is time t, and the state variables (S_M, S_P, $E_{1,M}, \ldots, E_{5,M}$, $E_{1,P}, \ldots, E_{5,P}$, $E_{2,Q}, \ldots, E_{5,Q}$, A_M, A_P, A_Q, I_M, I_P, I_Q, H_U, D, R_U, $V_1, \ldots, V_6$, $S_{V,1}, \ldots, S_{V,4}$, E_V, A_V, I_V, H_V, and R_V) represent 40 (sub)populations (Appendix Table 1), which change over time. Thus, each ODE in Equations (1)–(28) defines the time-rate of change of a population, i.e., the time-rate of change of a state variable. Note that Equations (5), (6), (8) and (19) define 4, 4, 3, and 5 ODEs of the model, respectively. The model is formulated such that S_0, the total population, is a constant. Thus, the model does not account for birth, death for reasons other than COVID-19, immigration, or emigration.

The initial condition associated with Equations (1)–(28) is taken to be $S_M(t_0) = S_0$, $I_M(t_0) = I_0 = 1$, and all other populations (S_P, $E_{1,M}, \ldots, E_{5,M}$, $E_{1,P}, \ldots, E_{5,P}$, $E_{2,Q}, \ldots, E_{5,Q}$, A_M, A_P, A_Q, I_P, I_Q, H_U, D, R_U, $V_1, \ldots, V_6$, $S_{V,1}, \ldots, S_{V,4}$, E_V, A_V, I_V, H_V, and R_V) are equal to 0. Recall

that the parameter S_0 denotes the total region-specific population size. Thus, we assume that the entire population is susceptible at the start of the local epidemic at time $t = t_0$>0, where time $t = 0$ corresponds to 0000 hours (midnight) on January 21, 2020. The parameter I_0 denotes the number of infectious symptomatic persons at the start of the regional epidemic.

In the model, the parameters β, k_L, k_Q, j_Q, c_A, c_I, c_H, and k_V are positive-valued rate constants (all with units of d^{-1}), and the parameters m_b, m_h, f_A, f_H, f_R, $f_0 \geq f_1$, $f_1 \geq f_2$, and f_2 are (dimensionless) fractions. Brief definitions of parameters are given in Tables 1 and 2.

In the model, the quantities $\phi_M(t,\rho)$, $\phi_P(t,\rho)$, and $\phi_V(t)$ are functions of (time-dependent) state variables (as defined below), which represent the population of infectious persons who are mixing freely (i.e., not practicing social distancing), the population of infectious persons who are practicing social distancing (i.e., adopting disease-avoiding behaviors), and the population of persons eligible for vaccination, respectively. The quantities $\phi_M(t,\rho)$ and $\phi_P(t,\rho)$ are also functions of $\rho \equiv (\rho_E, \rho_A)$, where ρ_E (ρ_A) is a dimensionless ratio representing the infectiousness of persons in the incubation phase of infection (the infectiousness of asymptomatic persons in the immune clearance phase of infection) relative to the infectiousness of symptomatic persons with the same social-distancing behavior. The quantity $\phi_V(t)$ represents the population of persons eligible for vaccination.

$$\phi_M(t,\rho) = I_M + I_V + \rho_E\left(E_{2,M} + E_{3,M} + E_{4,M} + E_{5,M} + E_V\right) + \rho_A(A_M + A_V) \tag{29}$$

$$\phi_P(t,\rho) = I_P + \rho_E\left(E_{2,P} + E_{3,P} + E_{4,P} + E_{5,P}\right) + \rho_A A_P \tag{30}$$

$$\phi_V(t) = S_M + S_P + \sum_{i=1}^{5}\left(E_{i,M} + E_{i,P}\right) + A_M + A_P + R_U \tag{31}$$

608 The state variables that appear in these equations represent time-varying populations. Recall that
609 state variables are defined in Appendix Table 1.

610 In the model, the quantities $U_\sigma(t)$, $U_{\theta_1}(t)$, and $U_{\theta_2}(t)$ are unit step functions. The values
611 of these functions change from 0 to 1 at the times indicated by the subscripts: σ, the onset time of
612 the initial social-distancing period; θ_1, the takeoff time of SARS-CoV-2 variant Alpha; and θ_2,
613 the takeoff time of SARS-CoV-2 variant Delta.

$$U_\sigma(t) = \begin{cases} 0 & t < \sigma \\ 1 & t \geq \sigma \end{cases} \tag{32}$$

$$U_{\theta_1}(t) = \begin{cases} 0 & t < \theta_1 \\ 1 & t \geq \theta_1 \end{cases} \tag{33}$$

$$U_{\theta_2}(t) = \begin{cases} 0 & t < \theta_2 \\ 1 & t \geq \theta_2 \end{cases} \tag{34}$$

614 As indicated in Appendix Figure 1, transitions from S_M to S_P, for example, become possible at
615 time $t = \sigma$, transitions from $S_{V,2}$ to E_V become possible at time $t = \theta_1$, and transitions from $S_{V,3}$
616 to E_V become possible at time $t = \theta_2$.

617 In the model, the quantities $P_\tau(t)$, and $\Lambda_\tau(t)$ are step functions that characterize changes
618 in social distancing. The value of $P_\tau(t)$ determines a setpoint steady-state fraction of susceptible
619 persons who are practicing social distancing. The value of $\Lambda_\tau(t)$ determines a time scale for
620 approach to the setpoint steady state. Changes in the values of $P_\tau(t)$ and $\Lambda_\tau(t)$ occur
621 coordinately. These changes occur at times $t = \sigma, \tau_1, \ldots, \tau_n$, where n is the number of distinct

social-distancing periods beyond an initial social-distancing period. Initially, we took $n = 7$ (i.e., 8 total social-distancing stages). The value of n is decremented by 1 (at an inferred time) if $n \leftarrow n - 1$ is determined to be admissible by a model-selection procedure, which is described below. It should be noted that $p_0, p_1, \ldots, p_n$ are parameters of $P_\tau(t)$ and that $\lambda_0, \lambda_1, \ldots, \lambda_n$ are parameters of $\Lambda_\tau(t)$. These parameters determine the non-zero values of the step functions over different periods. For example, p_1 is the value of $P_\tau(t)$ and λ_1 is the value of $\Lambda_\tau(t)$ for the period $t \in [\tau_1, \tau_2)$.

$$P_\tau(t) = \begin{cases} p_0 & \sigma \leq t < \tau_1 \\ p_1 & \tau_1 \leq t < \tau_2 \\ \vdots & \vdots \\ p_n & \tau_n \leq t < \infty \end{cases} \tag{35}$$

$$\Lambda_\tau(t) = \begin{cases} \lambda_0 & \sigma \leq t < \tau_1 \\ \lambda_1 & \tau_1 \leq t < \tau_2 \\ \vdots & \vdots \\ \lambda_n & \tau_n \leq t < \infty \end{cases} \tag{36}$$

The values of $P_\tau(t)$ and $\Lambda_\tau(t)$ are 0 for $t < \sigma$.

In the model, the quantity $\mu(t)$ is a piecewise linear interpolant to a function $\tilde{\mu}(t)$ that characterizes the current rate of vaccination. The value of $\tilde{\mu}(t)$ is determined by the empirical daily rate of vaccination, and thus, can vary from day to day. Daily vaccination data were extracted from the Covid Act Now database using the Covid Act Now Data API [1]. We will use μ_i to refer to the value of $\tilde{\mu}(t)$ for $t \in [t_i, t_{i+1})$, where time t_i corresponds to midnight on the ith day after January 21, 2020.

$$\tilde{\mu}(t) = \mu_i \text{ for } t \in [t_i, t_{i+1}) \tag{37}$$

Settings for μ_i were made such that $\mu_i S_0 \times 1$ d is the number of vaccinations completed in the nearest past 1-d period according to Covid Act Now data.

In the model, the quantity $Y_\theta(t)$ is a step function that quantifies how disease transmissibility increases upon emergence of SARS-CoV-2 variants Alpha and Delta. Initially, $Y_\theta(t) = 1$. The value of $Y_\theta(t)$ is increased (by an inferred factor greater than 1 at an inferred time, θ_1 or θ_2) if the change is determined to be admissible by a model-selection procedure, which is described below. It should be noted that y_1 and y_2 are parameters of $Y_\theta(t)$. These parameters determine the values of the step function $Y_\theta(t)$ over different periods: y_1 is the value of $Y_\theta(t)$ for the period $t \in [\theta_1, \theta_2)$ and y_2 is the value of $Y_\theta(t)$ for the remaining period of concern (with Delta as the dominant circulating viral strain).

$$Y_\theta(t) = \begin{cases} y_0 & \theta_0 \le t < \theta_1 \\ y_1 & \theta_1 \le t < \theta_2 \\ \vdots & \vdots \\ y_m & \theta_m \le t < \infty \end{cases} \tag{38}$$

where m is the number of viral variants that have emerged up to the current time, $\theta_0 \equiv t_0$, and $y_0 \equiv 1$. Here, we consider $m = 2$.

Equations of the Auxiliary Measurement Model

As in the study of Lin et al. [2], we assumed that only symptomatic persons are detected in testing. The accumulation of symptomatic persons is governed by

$$\frac{dC_S}{dt} = (1 - f_A)\left[k_L\left(E_{5,M} + E_{5,P} + E_{5,Q}\right) + \left(\frac{k_L}{5}\right)E_V\right] \tag{39}$$

where $C_S(t)$ is the cumulative number of symptomatic persons (cases) at time t. Here, unlike in the study of Lin et al. [2], the expression for $C_S(t)$ accounts for exposed persons in quarantine.

Initially, $C_S = 0$. We numerically integrated Appendix Equation (39) together with the ODEs of the compartmental model. From the trajectory for C_S, we derive a prediction for the expected number of new COVID-19 cases reported on calendar date $\mathcal{D}_{\mathrm{i}}$, $I(t_i, t_{i+1})$, using the following equation:

$$I(t_i, t_{i+1}) = f_D[C_S(t_{i+1}) - C_S(t_i)] \tag{40}$$

where f_D is an adjustable region-specific parameter characterizing the time-averaged fraction of symptomatic cases detected and reported, t_i corresponds to midnight on the ith day after January 21, 2020, and $t_{i+1} - t_i$ is the reporting interval (1 d). We compare $I(t_i, t_{i+1})$ to δC_i, the number of new cases reported on calendar date $\mathcal{D}_{\mathrm{i}}$.

Definition of the Likelihood Function

Bayesian inference relies on the definition of a likelihood, which here serves the purpose of assessing the compatibility of available surveillance data with adjustable (free) parameter values. Let us use $\{\delta C_i\}_{i=0}^{d}$ to denote the daily case reporting data available between 0 and d days after midnight on January 21, 2020 (the date of the first case report in the US) and let $D = \{\delta C_i\}_{i=0}^{d}$. Let us use $\theta_F(n, m)$ to denote the set of adjustable (free) parameter values. The number of adjustable parameters, $|\theta_F|$, depends on n, the number of social-distancing periods considered beyond an initial social-distancing period, and m, the number of SARS-CoV-2 variants under consideration. As in the study of Lin et al. [2], we assume that δC_i, the number of new COVID-19 cases detected over a 1-d period and reported on calendar date $\mathcal{D}_{\mathrm{i}}$ for a given region, is a random variable and its expected value follows a model-derived deterministic trajectory given by $I(t_i, t_{i+1})$ (Equation 40). We assume that day-to-day fluctuations in the random variable are independent and characterized by a negative binomial distribution $\mathrm{NB}(r, q_i)$,

674 which has two parameters, $r > 0$ and $q_i \in (0,1)$. Note that $\mathbb{E}[\mathrm{NB}(r, q_i)] = r(1 - q_i)/q_i$. We
675 assume that this distribution has the same dispersion parameter r across all case reports. With
676 these assumptions, we arrive at the following likelihood function:

$$\mathcal{L}\left(\theta_F(n,m); \{\delta C_i\}_{i=0}^{d}\right) = \prod_{i=0}^{d} \mathcal{L}_i(\theta_F(n,m); \delta C_i) \tag{41}$$

677 where

$$\mathcal{L}_i(\theta_F(n,m); \delta C_i) = \mathrm{nbinom}(\delta C_i; r, q_i) = \binom{\delta C_i + r - 1}{\delta C_i - 1} q_i^r (1 - q_i)^{\delta C_i} \tag{42}$$

678 and

$$q_i = \frac{r}{r + I(t_i, t_{i+1})}. \tag{43}$$

679 In these equations, i is an integer indicating the date $\mathcal{D}_i$ and period (t_i, t_{i+1}); $\mathrm{nbinom}(\delta C_i; r, q_i)$
680 is the probability mass function of the negative binomial distribution $\mathrm{NB}(r, q_i)$, and $\theta_F(n,m) =$
681 $\{t_0, \beta, \sigma, \tau_1, \ldots, \tau_n, p_0, p_1, \ldots, p_n, \lambda_0, \lambda_1, \ldots, \lambda_n, \theta_1, \ldots, \theta_m, y_1, \ldots, y_m, f_D, r\}$ for $n \geq 1$ and $m \geq 1$;
682 $\theta_F(0,0) = \{t_0, \beta, p_0, \lambda_0, f_D, r\}$.

683 **Parameters**

684 Each model parameter is briefly described in Tables 1–3. These parameters have either
685 fixed values or adjustable values (i.e., values inferred from surveillance data). The fixed values
686 may be universal (i.e., applicable to all MSAs of interest) or MSA-specific. All inferred
687 parameter values are MSA-specific. In addition, the measurement model (Appendix Equations
688 39 and 40) has one adjustable MSA-specific parameter, f_D, and the likelihood function

(Appendix Equations 41–43) has one adjustable MSA-specific parameter, r. Values of the other likelihood parameters, $q_0, \ldots, q_d$, are constrained and are determined using Appendix Equation 43.

The model shares $19 + 3n$ parameters with the model of Lin et al. [2], including parameters that define the initial condition (t_0, I_0, and S_0). (Recall that n is the number of social-distancing periods being considered beyond the initial social-distancing period.) The shared parameters are t_0, I_0, S_0, β, σ, $\tau_1, \ldots, \tau_n$, $p_0, \ldots, p_n$, $\lambda_0, \ldots, \lambda_n$, ρ_A, ρ_E, m_b, f_A, f_H, f_R, k_L, k_Q, j_Q, c_A, c_H, and c_I. As in the study of Lin et al. [2], we inferred MSA-specific values for the following parameters: t_0, β, σ, $p_0, \ldots, p_n$, and $\lambda_0, \ldots, \lambda_n$. We also inferred MSA-specific values for $\tau_1, \ldots, \tau_n$ provided that $n \geq 1$. As in the study of Lin et al. [2], the remaining 14 parameters shared between the old and new models (I_0, S_0, ρ_A, ρ_E, m_b, f_A, f_H, f_R, k_L, k_Q, j_Q, c_A, c_H, and c_I) were taken to have fixed values, and we adopted the settings of Lin et al. [2] for these parameters (Table 3). These settings are universal except for the setting for S_0, the total population, which is MSA-specific.

Our extension of the model of Lin et al. [2] introduces $5 + 2(m + 1) + (d + 1)$ parameters, where m (= 0, 1 or 2) is the number of SARS-CoV-2 variants being considered and d is the number of days since January 21, 2020: $\theta_0, \ldots, \theta_m$, $y_0, \ldots, y_m$, m_h, f_0, f_1, f_2, k_V, and $\mu_0, \ldots, \mu_d$. The θ and y parameters are variant takeover times and transmissibility factors, respectively, except that the value of θ_0 is defined as t_0 and the value of y_0 is defined as 1. The Alpha transmissibility factor y_1, the Alpha takeoff time θ_1, the Delta transmissibility factor y_2, and the Delta takeoff time θ_2 were inferred for each MSA with $m = 2$ (cf. Table 1). The transmissibility factors were each constrained to be greater than or equal to 1. The settings for

$\mu_0, \ldots, \mu_d$ are empirical and MSA-specific. Each μ_i is set such that $\mu_i S_0 \times 1$ d is the number of vaccinations completed over the past 1-d period nearest to the ith day after January 21, 2020. As noted earlier, the number of completed vaccinations was obtained for each MSA from Covid Act Now using the Covid Act Now Data API [1]. In the spreadsheet accessed daily, the 'metrics.vaccinationsCompletedRatio' column gives the percentage of the total population that has received the recommended number of doses: one dose for Ad26.CoV2.S (Janssen, Johnson & Johnson) or two doses for mRNA-1273 (Moderna) and BNT162b2 (Pfizer-BioNTech). As a simplification, we considered all completed vaccinations to be equivalent. The parameters m_h, f_0, f_1, f_2, and k_V were assigned fixed universal estimates (Table 3). Each of these estimates is explained below.

The rate constant k_V characterizes the rate of transition out of compartment V_i for $i = 1, \ldots, n_V$. Recall that, in the model, susceptible persons enter V_1 upon vaccination (Figure 1, Appendix Figure 1). The values of n_V $(= 6)$ and k_V $(= 0.3\ \mathrm{d}^{-1})$ were selected so that the time a person spends in $V_1, \ldots, V_{n_V}$, which we will denote as t_V, is distributed approximately the same as $\tilde{t}_V$, the waiting time between vaccination of a previously uninfected person and detection of vaccine-induced SARS-CoV-2-specific IgG antibodies [3] (Appendix Figure 2). According to the model, the time that a person spends in $V_1, \ldots, V_{n_V}$ is distributed according to the probability density function $f(t_V; n_V, k_V) = k_V^{n_V} t_V^{n_V - 1} e^{-k_V t_V} / (n_V - 1)!$, i.e., t_V is Erlang distributed with shape parameter $n_V = 6$ and rate parameter $k_V = 0.3\ \mathrm{d}^{-1}$. As can be seen in Appendix Figure 2, the cumulative distribution function of this Erlang distribution reasonably captures the empirical cumulative distribution of waiting times observed in the longitudinal study of Korodi et al. [3]. Thus, in the model, passage through $V_1, \ldots, V_6$ with rate constant $k_V = 0.3\ \mathrm{d}^{-1}$ accounts for the

733 variable and significantly non-zero amount of time required for development of a protective
734 antibody response after vaccination.

735 The parameters $f_0 > f_1$, $f_1 > f_2$, and f_2 are fractions that characterize the average
736 effectiveness of vaccines used in the US and that determine the sizes of (mutually exclusive)
737 subpopulations of vaccinated persons having different susceptibilities to productive infection
738 (i.e., an infection that can be transmitted to others): $S_{V,1}$, $S_{V,2}$, $S_{V,3}$, and $S_{V,4}$ (Figure 1, Appendix
739 Figure 1). We assume that persons in the $S_{V,1}$ subpopulation are susceptible to productive
740 infection by any of the viral strains considered, and in contrast, we assume that persons in the
741 $S_{V,4}$ subpopulation are susceptible to productive infection by none of the viral strains considered.
742 Persons in the $S_{V,2}$ subpopulation are taken to be susceptible to productive infection by the Alpha
743 and Delta variants but not viral strains in circulation before the emergence of Alpha. Persons in
744 the $S_{V,3}$ subpopulation are taken to be susceptible to productive infection by the Delta variant but
745 not the Alpha variant or viral strains in circulation before the emergence of Alpha. The quantity
746 $1 - f_0$ defines the fraction of vaccinated persons who enter the $S_{V,1}$ subpopulation after exiting
747 V_6, the quantity $f_0 - f_1$ defines the fraction of vaccinated persons who enter the $S_{V,2}$
748 subpopulation after exiting V_6, the quantity $f_1 - f_2$ defines the fraction of vaccinated persons
749 who enter the $S_{V,3}$ subpopulation after exiting V_6, and f_2 defines the fraction of vaccinated
750 persons who enter the $S_{V,4}$ subpopulation after exiting V_6. We take f_0 to characterize vaccine
751 effectiveness before the emergence of Alpha. According to Thompson et al. [4], vaccine
752 effectiveness was initially 90%. Thus, we set $f_0 = 0.9$. We take f_1 to characterize vaccine
753 effectiveness after the emergence of Alpha but before the emergence of Delta. According to
754 Puranik et al. [5], in May 2021, vaccine effectiveness was 81%. Thus, we set $f_1 = 0.81$. We take
755 f_2 to characterize vaccine effectiveness after the emergence of Delta. According to Tang et al.

[6], the effectiveness of two doses of the Pfizer-BioNTech vaccine (BNT162b2) against Delta is 53.5% and the effectiveness of two doses of the Moderna vaccine (mRNA-1273) against Delta is 84.8%. Taking the average of these figures, we set $f_2 = 0.69$.

The parameter m_h characterizes the reduced risk of severe disease for a vaccinated person in the case of a breakthrough infection. We set $m_h = 0.04$, i.e., we assumed that there is a 25-fold reduction in the risk of severe disease for infected persons who have been vaccinated, which is consistent with the observations of Lopez Bernal et al. [7].

Notable New Modeling Assumptions

It should be noted that we treat the incubation period for newly infected (exposed) vaccinated persons differently than for newly infected (exposed) unvaccinated persons (Figure 1, Appendix Figure 1). For unvaccinated persons, as in the study of Lin et al. [2], we divide exposed persons in the incubation period of infection into five subpopulations: $E_{1,M}, \ldots, E_{5,M}$ for exposed persons who are mixing (i.e., persons who are not practicing social distancing), $E_{1,P}, \ldots, E_{5,P}$ for exposed persons who are practicing social distancing, and $E_{1,Q}, \ldots, E_{5,Q}$ for exposed quarantined persons. Persons move through the five stages of the incubation period sequentially. In contrast, as a simplification, for vaccinated persons, we consider only a single exposed population: E_V. We take persons to exit E_V with rate constant $k_L/5$ (Appendix Figure 1). With this choice, the duration of the incubation period of infection is the same, on average, for both vaccinated and unvaccinated persons. The average duration is $5/k_L$ (about 5 d) in both cases. The difference is that the duration of the incubation period is Erlang distributed for unvaccinated persons, as discussed by Lin et al. [2], but exponentially distributed for vaccinated persons.

As indicated in Equation (29), we take vaccinated persons with productive infections to be equally as infectious as unvaccinated persons.

As noted earlier, we take all vaccinated persons to be mixing (i.e., to not be practicing social distancing). Thus, populations of infected vaccinated persons (E_V, I_V, and A_V) contribute to $\phi_M(t)$ (Appendix Equation 29) but not $\phi_P(t)$ (Appendix Equation 30).

As indicated in Appendix Equation 31, we consider pre-symptomatic exposed and asymptomatic unvaccinated persons to be eligible for vaccination and, thus, these persons contribute to the consumption of vaccine doses (i.e., these persons account for a portion of the number of completed vaccinations on a given day i, $\mu_i S_0 \times 1$ d). However, we do not move these persons to vaccinated compartments. The reason is that exposed and asymptomatic persons are expected to develop immunity faster through recovery from infection (i.e., movement to R_U) than from vaccination.

As indicated in Appendix Equation 31, we do not consider symptomatic, quarantined, severely ill and hospitalized/isolated-at-home, and deceased persons to be eligible for vaccination.

Inference Approach

Recall that θ_F denotes the set of all adjustable parameters. As in the study of Lin et al. [2], for each MSA, we inferred MSA-specific adjustable parameter values θ_F using all MSA-specific surveillance data available up to a specified day of inference $\mathcal{D}_{\mathrm{d}}$ (i.e., the dth day after January 21, 2020). We took a Bayesian inference approach, meaning that, for a given dataset, we generated parameter posterior samples (a collection of θ_F's) through Markov chain Monte Carlo (MCMC) sampling. The parameter posterior samples provide a probabilistic characterization of

the adjustable parameter values consistent with the dataset used in inference. By drawing samples from the parametric posterior distribution, we generated a posterior predictive distribution for $I(t_i, t_{i+1})$ for each i of interest. We considered all days from January 21, 2020 to October 31, 2021. In other words, for each i of interest, a prediction for $I(t_i, t_{i+1})$ was generated for each of many θ_F's drawn randomly (with uniform probability) from the parametric posterior distribution. The resulting distribution of $I(t_i, t_{i+1})$ values is the posterior predictive distribution for $I(t_i, t_{i+1})$. Recall that $I(t_i, t_{i+1})$ is given by Appendix Equation 40 and corresponds to $\mathbb{E}[\delta C_i]$, the expected number of new COVID-19 cases detected over a 1-d surveillance interval and reported for the ith day after January 21, 2020. Observation noise was injected into the posterior predictive distributions by replacing each sampled value for $I(t_i, t_{i+1})$ with $X_i \sim \mathrm{NB}(r, q_i)$, where r is a member of the sampled set of parameter values θ_F used to generate the prediction of $I(t_i, t_{i+1})$ and q_i is given by Equation 43.

According to Bayes' theorem, given surveillance data $D = \{\delta C_i\}_{i=0}^{d}$, the parametric posterior is given as

$$\mathbb{P}\{\theta_F|D\} = \frac{\mathbb{P}\{D|\theta_F\}\,\mathbb{P}\{\theta_F\}}{Z} \tag{44}$$

where $\mathbb{P}\{\theta_F\}$ is the prior (which is formulated to capture knowledge of θ_F external to D or to express lack of such knowledge), $\mathbb{P}\{D|\theta_F\}$ is the likelihood defined by Appendix Equations 41–43, and Z is a normalizing constant. We assumed a proper uniform prior, i.e., for each adjustable parameter, we assumed that all values between specified lower and upper bounds are equally likely before consideration of D. We used the same bounds as in the study of Lin et al. [2]. Then we used an adaptive MCMC (aMCMC) algorithm [8] to generate samples from $\mathbb{P}\{D|\theta_F\}\,\mathbb{P}\{\theta_F\}$,

which is proportional to $\mathbb{P}\{\theta_F|D\}$. Thus, the relative probabilities of parameter sets θ_F according to $\mathbb{P}\{\theta_F|D\}$ are correctly represented by the samples.

Specifically, the adaptive MCMC algorithm [8] generates samples from the multivariate parametric posterior for adjustable model parameters (t_0, β, and parameters for variant emergence and social distancing), the measurement model parameter f_D, and the likelihood parameter r (Tables 1 and 2). This algorithm is available within the PyBioNetFit software package [9]. Use of the algorithm was performed as described by Lin et al. [2]. The report of Neumann et al. [9] includes helpful general usage advice, which was followed in this study. Inference jobs were executed on a computer cluster.

Each inference was conditioned on the compartmental model of Figure 1 (Appendix Equations 1–38), settings for the structural parameters m (the number of SARS-CoV-2 variants under consideration) and n (the number of social-distancing periods under consideration beyond an initial social-distancing period), the measurement model (Appendix Equations 39 and 40), and fixed parameter estimates (Tables 1 and 2), including empirical daily *per-capita* vaccination rates (i.e., the settings for μ_i in Appendix Equation 37). We assumed a proper uniform prior for each adjustable parameter [2] and a negative binomial likelihood function (Appendix Equations 41–43). Use of proper uniform priors means that MAP estimates are maximum likelihood estimates (MLEs). In each inference, the data entering the likelihood function, $D = \{\delta C_i\}_{i=0}^{d}$ (Appendix Equation 41), were MSA-specific daily reports of newly detected COVID-19 cases available up to the date of inference $\mathcal{D}_{\mathrm{d}}$ (i.e., the d-th day after January 21, 2020). Thus, all inferences are region-specific and time-dependent.

Use of Model Selection to Determine Intervals of Step Functions

Variant takeover times, $\theta = (\theta_1, \theta_2)$, and start times of social-distancing periods, $\tau = (\sigma, \tau_1, \ldots, \tau_n)$, were inferred from data; however, changes of the associated time-dependent step functions, $Y_\theta(t)$, $P_\tau(t)$, and $\Lambda_\tau(t)$, were introduced only when an increase in model complexity was deemed to be justified. Each decision to introduce variant takeover or start of a new social-distancing period (beyond the initial period) was made using a model-selection procedure, which is described below. It should be noted that y_1 and y_2 are parameters of $Y_\theta(t)$, $p_0, p_1, \ldots, p_n$ are parameters of $P_\tau(t)$, and $\lambda_0, \lambda_1, \ldots, \lambda_n$ are parameters of $\Lambda_\tau(t)$. These parameters determine the values of the step functions over different periods. For example, for $n \geq 1$, p_1 is the value of $P_\tau(t)$ and λ_1 is the value of $\Lambda_\tau(t)$ for the period $t \in [\tau_1, \tau_2)$. Similarly, y_1 is the value of $Y_\theta(t)$ for the period $t \in [\theta_1, \theta_2)$, and y_2 is the value of $Y_\theta(t)$ for the period $t \in [\theta_2, t_{\text{final}})$, where t_{final} corresponds to the date of inference (October 31, 2021).

We started with a setting of $n = 7$ for each MSA of interest (i.e., 8 total social-distancing stages). To determine if n could be reduced, we conducted so-called "parsimony checks". In a parsimony check, 100 MLE curves, each constituting a fit to the data, were generated via optimization jobs (started at 100 randomly selected locations in parameter space). The total number of social-distancing stages $n + 1$ in the model was 1 less than for the current proposed best fit. Each of the 100 fits was then visually inspected to check whether or not the following criteria held: 1) the quality of fit is acceptable (i.e., comparable to what is obtained with the current proposed best fit); 2) Alpha and Delta surges (identified by sequencing data) are explained at least partly by increased transmissibility; 3) social-distancing setpoint parameter values are feasible; 4) social-distancing changes proximal to an Alpha or Delta surge (if any) occur only after an increase in transmissibility. If one or more of these conditions was not satisfied, we accepted the proposed best fit as the most parsimonious fit to the data. If all of the

conditions held, we had a new proposed best fit, and the parsimony check was repeated for a model with one less social-distancing stage.

Simulations

After specification of parameter values (Tables 1–3), we used the SciPy (https://www.scipy.org) interface to LSODA [11] to numerically integrate the system of coupled ODEs consisting of the 40 ODEs of the compartmental model and the 1 ODE of the measurement model (Appendix Equations 1–39). The initial condition was defined by settings for t_0, I_0, and S_0 (Tables 1–3). Integration combined with use of Appendix Equation 40 yielded a prediction of the expected number of new cases detected for each 1-d surveillance period of interest in the past or future: $I(t_i, t_{i+1})$, where t_i corresponds to midnight on the ith day after January 21, 2020. To account for randomness in case detection and reporting, we replaced $I(t_i, t_{i+1})$ with $X_i \sim \mathrm{NB}(r, q_i)$, where q_i is given by Appendix Equation 43.

Appendix References

[1] Covid Act Now. US COVID risk and vaccine tracker. 2021 [cited 2021 Sep 29] https://covidactnow.org/

[2] Lin YT, Neumann J, Miller EF, Posner RG, Mallela A, Safta C, Ray J, Thakur G, Chinthavali S, Hlavacek WS. Daily forecasting of regional epidemics of Coronavirus Disease with Bayesian uncertainty quantification, United States. Emerg Inf Dis. 2021;27:767–78. https://doi.org/10.3201/eid2703.203364

[3] Korodi M, Rákosi K, Jenei Z, Hudák G, Horváth I, Kákes M, et al. Longitudinal determination of mRNA-vaccination induced strongly binding SARS-CoV-2 IgG antibodies in a cohort of healthcare workers with and without prior exposure to the novel

887 coronavirus. Vaccine. 2022;40:37: 5445–5451.
888 https://doi.org/10.1016/j.vaccine.2022.07.040
889 [4] Thompson MG, Burgess JL, Naleway AL, Tyner HL, Yoon SK, Meece J, et al. Interim
890 estimates of vaccine effectiveness of BNT162b2 and mRNA-1273 COVID-19 vaccines
891 in preventing SARS-CoV-2 infection among health care personnel, first responders, and
892 other essential and frontline workers—eight U.S. locations, December 2020–March 2021.
893 MMWR Morb Mortal Wkly Rep. 2021;70:495–500.
894 http://dx.doi.org/10.15585/mmwr.mm7013e3
895 [5] Puranik A, Lenehan PJ, Silvert E, Niesen MJM, Corchado-Garcia J, O'Horo JC, et al.
896 Comparison of two highly-effective mRNA vaccines for COVID-19 during periods of
897 Alpha and Delta variant prevalence. [cited 2021 Oct 8]
898 https://www.medrxiv.org/content/10.1101/2021.08.06.21261707v3
899 [6] Tang P, Hasan MR, Chemaitelly H, Yassine HM, Benslimane FM, Al Khatib HA, et al.
900 BNT162b2 and mRNA-1273 COVID-19 vaccine effectiveness against the SARS-CoV-2
901 Delta variant in Qatar. Nat Med. 2021;27:2136–43.
902 https://www.nature.com/articles/s41591-021-01583-4
903 [7] Lopez Bernal J, Andrews N, Gower C, Gallagher E, Simmons R, Thelwall S, et al.
904 Effectiveness of Covid-19 Vaccines against the B.1.617.2 (Delta) variant. N Engl J Med.
905 2021;385:585–94. https://doi.org/10.1056/NEJMoa2108891
906 [8] Andrieu C, Thoms J. A tutorial on adaptive MCMC. Stat Comput. 2008;18:343–73.
907 https://doi.org/10.1007/s11222-008-9110-y
908 [9] Neumann J, Lin YT, Mallela A, Miller EF, Colvin J, Duprat AT, Chen Y, Hlavacek WS,
909 Posner RG. Implementation of a practical Markov chain Monte Carlo sampling algorithm

in PyBioNetFit. Bioinformatics. 2022;38:1770–2. https://doi.org/10.1093/bioinformatics/btac004

[10] Burnham KP, Anderson DR. Multimodal inference: understanding AIC and BIC in model selection. Sociol Methods Res. 2016;33:261–304. https://doi.org/10.1177/0049124104268644

[11] Hindmarsh AC. ODEPACK, a systematized collection of ODE solvers. In Stepleman RS, editor. Scientific computing: applications of mathematics and computing to the physical sciences. Amsterdam: North-Holland Publishing Company; 1983. p. 55–64.

Appendix Table 1. State variables of the compartmental model

State variable (population)	Description
S_M	Population of susceptible unvaccinated persons who are mixing (i.e., not practicing social distancing)
S_P	Population of susceptible unvaccinated persons who are practicing social distancing
$S_{V,1}$	Population of vaccinated unexposed persons who developed an immune response to vaccination that does not protect against productive infection by ancestral strains or the Alpha and Delta variants
$S_{V,2}$	Population of vaccinated unexposed persons who developed an immune response to vaccination that protects against productive infection by ancestral strains but not the Alpha or Delta variants
$S_{V,3}$	Population of vaccinated unexposed persons who developed an immune response to vaccination that protects against productive infection by ancestral strains and the Alpha variant but not the Delta variant
$S_{V,4}$	Population of vaccinated unexposed persons who developed an immune response to vaccination that protects against productive infection by ancestral strains and the Alpha and Delta variants
V_i $(i = 1, \dots, 6)$	Population of vaccinated persons in the ith stage of immune response to vaccination
$E_{i,M}$ $(i = 1, \dots, 5)$	Population of exposed unvaccinated persons in the ith stage of the incubation period of infection and who are mixing
$E_{i,P}$ $(i = 1, \dots, 5)$	Population of exposed unvaccinated persons in the ith stage of the incubation period of infection and who are practicing social distancing
$E_{i,Q}$ $(i = 2, \dots, 5)$	Population of exposed unvaccinated persons in the ith stage of the incubation period of infection and who are quarantined
E_V	Population of vaccinated persons in the incubation period of a productive infection (i.e., an infection that can be transmitted to others)

A_M	Population of asymptomatic unvaccinated persons who are in the immune clearance phase of infection and who are mixing
A_P	Population of asymptomatic unvaccinated persons who are in the immune clearance phase of infection and who are practicing social distancing
A_Q	Population of asymptomatic unvaccinated persons who are in the immune clearance phase of infection and who are quarantined
A_V	Population of asymptomatic vaccinated persons who are in the immune clearance phase of a productive infection (i.e., an infection that can be transmitted to others)
I_M	Population of infectious, symptomatic, and unvaccinated persons with mild disease who are mixing
I_P	Population of infectious, symptomatic, non-vaccinated, and infectious persons with mild disease who are practicing social distancing
I_Q	Population of infectious, symptomatic, and unvaccinated persons with mild disease who are quarantined
I_V	Population of infectious, symptomatic, and vaccinated persons with mild disease
R_U	Population of recovered unvaccinated persons
R_V	Population of recovered vaccinated persons
H_U	Population of unvaccinated persons with severe disease who are hospitalized or isolated at home
H_V	Population of vaccinated persons with severe disease who are hospitalized or isolated at home
D	Population of deceased persons

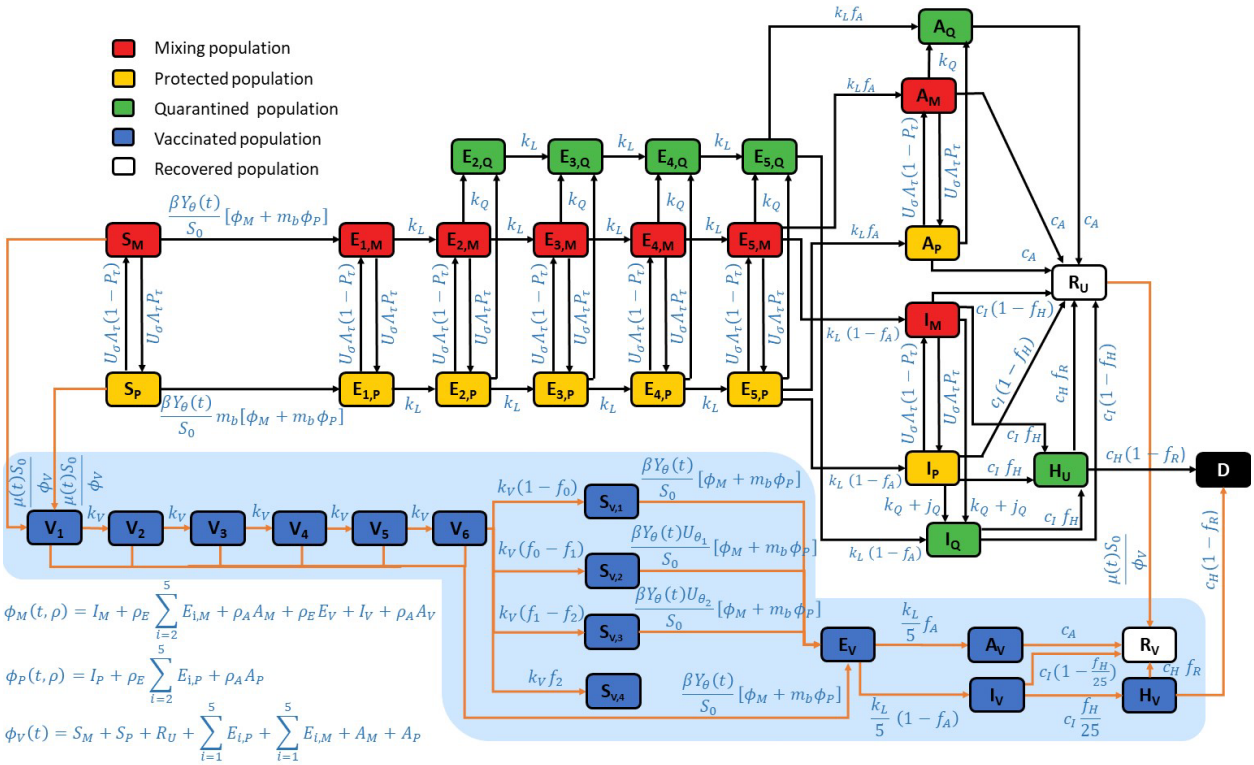

Appendix Figure 1. Expanded illustration of the new compartmental model. In the extended model, vaccination was considered by allowing susceptible and recovered persons to transition into a vaccinated compartment, either V_1 and R_V. Susceptible (recovered) persons who have completed vaccination move into the V_1 (R_V) compartment. The susceptible persons who move into V_1 are drawn from S_M (populated by susceptible persons who are mixing and unprotected by social distancing) and from S_P (populated by susceptible persons who are protected by social distancing). After susceptible persons enter V_1, they can move through a series of additional compartments (V_2 through V_6), which are included to capture the time needed for immunity to develop after completion of vaccination. We estimate that the time needed to acquire immunity after vaccination is approximately three weeks based on longitudinal studies of anti-spike protein IgG levels [3]. Persons who exit the V_6 compartment without becoming infected enter one of the following compartments: $S_{V,1}$, $S_{V,2}$, $S_{V,3}$, or $S_{V,4}$. Persons in $S_{V,1}$ are taken to remain susceptible

to productive infection by all SARS-CoV-2 strains of interest (Alpha, Delta, and ancestral strains). Persons in $S_{V,2}$ are taken to be susceptible to SARS-CoV-2 Alpha and Delta variants. Persons in $S_{V,3}$ are taken to be susceptible to Delta. Persons in $S_{V,4}$ are taken to be protected against all strains of interest. Infection of persons in $S_{V,3}$ is only allowed if Delta is present, i.e., at times $t > \theta_2$. Infection of persons in $S_{V,2}$ is only allowed if Alpha or Delta is present, i.e., at times $t > \theta_1$. Vaccinated persons in compartments V_1 through V_6 and compartment $S_{V,1}$ are allowed to become infected at any time, at which point they transition to compartment E_V, consisting of vaccinated persons who were exposed before development of vaccine-induced immunity. Persons in compartment $S_{V,2}$ are allowed to become infected if $t \geq \theta_1$. Similarly, persons in compartment $S_{V,3}$ are allowed to become infected if $t \geq \theta_2$. Possible outcomes for persons in E_V are taken to be the same as those for unvaccinated exposed persons; however, the incubation period is taken to be distinct. Persons in E_V can experience asymptomatic disease (upon entering A_V) or they can become symptomatic (upon entering I_V). Persons in A_V eventually recover, entering compartment R_V. Persons in I_V can progress to severe disease (upon entering H_V) or recover (upon entering R_V). Persons in H_V either recover (moving into R_V) or die (moving into D). Persons who have recovered from infection, in the R_U compartment, move directly into the R_V compartment upon vaccination. Persons in the R_U and R_V compartments are taken to have full immunity. The vaccination rate at which susceptible and recovered persons move into vaccinated compartments is updated daily for consistency with the empirical overall rate of vaccination, which we extract daily from the COVID Act Now Data API [1]. The relative values of the vaccination rate are set such that each person eligible for vaccination has the same probability of being vaccinated. All unvaccinated persons are taken to be eligible for vaccination except symptomatic persons (in compartments I_M and I_P), persons who are hospitalized or

958 severely ill at home (in compartment H), quarantined persons (in the various compartments
959 labeled with a Q subscript), and deceased persons (in compartment D). It should be noted that
960 asymptomatic, non-quarantined persons (in compartments A_M and A_P) and presymptomatic, non-
961 quarantined persons (in the E compartments) are taken to be eligible (and to influence the
962 vaccination rate constants) but, as a simplification, these persons are not explicitly tracked as
963 vaccinated or unvaccinated because each of these persons will eventually enter either the D
964 compartment or the R_U compartment, at which point they will have immunity. In the model, the
965 effects of SARS-CoV-2 variants are captured by a time-dependent dimensionless multiplier
966 $Y_\theta(t)$ of the rate constant β. This rate constant, which appears in Appendix Equations 1–4, 18–
967 22, and 24, determines the rate of disease transmission within the subpopulation unprotected by
968 social-distancing behaviors when $Y_\theta(t) = 1$. We take $Y_\theta(t) = 1$ for times $t < \theta_1$, i.e., for the
969 initial period of the COVID-19 pandemic in the US that we take to have started on January 21,
970 2020. We take $Y_\theta(t)$ to have the form of a step function with distinct values greater than 1 for
971 periods starting at $t = \theta_1$ and $\theta_{k+1} > \theta_k$ for $k = 1, \ldots, m$. Thus, the model allows for m distinct
972 periods of variant strain dominance delimited by a set of start times $\theta = \{\theta_1, \ldots, \theta_m\}$. We
973 considered $m = 2$. We assume that variants differ only in transmissibility.

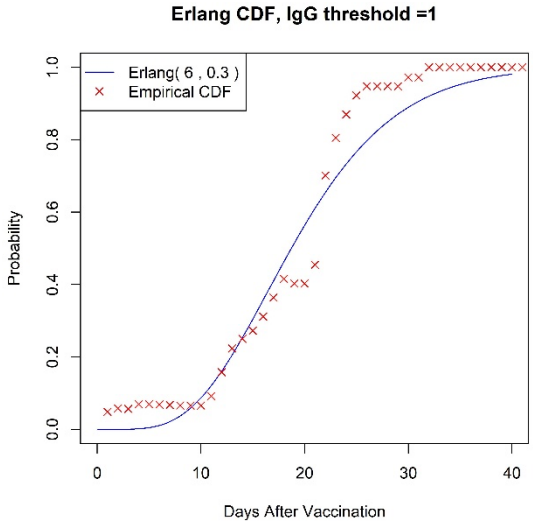

974

975 **Appendix Figure 2.** Comparison of an Erlang cumulative distribution function with shape
976 parameter $n_V = 6$ and rate parameter $k_V = 0.3\ \mathrm{d}^{-1}$ and the empirical cumulative distribution of
977 waiting times ($\tilde{t}_V$ values) observed in the longitudinal study of Korodi et al. [3]. The waiting
978 time $\tilde{t}_V$ is the time between vaccination of a previously uninfected person and detection of
979 vaccine-induced SARS-CoV-2-specific IgG antibodies.